Altered allostatic regulation of wakefulness and slow-wave-sleep spectral quality in mice with hypocretin (orexin) receptor 1 inactivation in noradrenergic cells

SHA LI[a], PAUL FRANKEN, AND ANNE VASSALLI[a]*

Center for Integrative Genomics, University of Lausanne, CH-1015 Lausanne, Switzerland

[a]Present address: Department of Physiology, University of Lausanne, CH-1005 Lausanne, Switzerland.

*Correspondence should be addressed to A.V. (anne.vassalli@unil.ch)

Abstract

The neuromodulators noradrenaline (NA) and hypocretins (Hcrt) both have major, but distinct, roles in implementing the brain circuit processing modes that define wakefulness and waking behaviors. The A6 NA cell group in the locus coeruleus (LC-NA) receives dense projections from the Hcrt cells of the hypothalamus, and acts as critical mediator of Hcrt-induced arousal. The range of behaviors relying on the Hcrt-to-LC-NA neuronal connection however remains undefined. We generated a conditionally inactivated allele of *Hcrtr1*, the Hcrt receptor gene expressed by LC-NA cells, and used a *Dbh-Cre* transgene to create mice with NA-specific *Hcrtr1* inactivation (*Hcrtr1*$^{Dbh\text{-}CKO}$ mice). Electrocortical activity (ECoG) of these mice was analyzed in distinct behavioral contexts, and contrasted to the one of *Cre*-less control littermates. While baseline waking was grossly normal albeit for enhanced activity in the slow-delta (δ) range, upon exposure to a novel environment, *Hcrtr1*$^{Dbh\text{-}CKO}$ mice displayed (i) a slowing of the waking ECoG, with enhanced δ and inter-δ/θ band activity, (ii) blunting of the θ rhythm and fast-γ activity, while (iii) β and slow-γ activities were enhanced. Moreover, locomotor and ECoG responses to sleep deprivation (SD) were markedly reduced. Surprisingly, while deficits in manually-enforced wakefulness resembled those following cage change (CC), spontaneous dark phase waking, and after providing nest material, were enhanced in θ and fast-γ oscillatory activities. Our data suggest that *Hcrtr1*$^{Dbh\text{-}CKO}$ mice are deficient in adaptive regulation of wakefulness in stress-associated conditions with electrocortical signs of decreased alertness and hippocampal θ activation. Furthermore, their waking θ and fast-γ ECoG power show concerted, but opposite, trends in stressful versus rewarding contexts. Finally, slow-wave-sleep (SWS) following SD and CC both showed a profound deficit in slow-δ activity, suggesting that Hcrt-to-NA signalling is critical in active waking to induce the homeostatic slow-δ rebound that characterizes ensuing SWS.

Introduction

Wakefulness is on one hand under circadian control, and on the other associated with adaptive responses to external stimuli. All these processes correlate with activity changes in cortical and subcortical neural networks that can be assessed in the electrocorticogram (ECoG). By neuromodulation of synaptic transmission throughout the brain, noradrenaline (NA) plays a major role in implementing the functional circuitry and processing modes that define the waking state.

A role of NA in regulation of cross-regional brain synchrony across cortex, striatum, thalamus and midbrain dopaminergic nuclei was suggested by using a mouse model of NA-depletion (Dzirasa et al. 2010). In these mice, NA depletion led to a profound disruption of coherence across these circuits, and to an altered behavior of the animal featuring transient hyperactivity, stereotypies and excessive grooming (Dzirasa et al. 2010). Modulation of NA signalling by pharmacological agents has also been shown to profoundly alter the waking ECoG spectral profile in rats (Sebban et al. 1999); (Berridge and Espana 2000).

The NA-producing cell group residing in the locus coeruleus (LC, or A6) produces approximately half of the brain NA content (Berridge 2008). Spontaneous tonic activity of LC-NA cells varies with behavioral states, and in wakefulness with arousal (Foote et al. 1980). Superimposed on the tonic discharge rate, exposure to novel and/or salient stimuli induces phasic bursts of activity in LC-NA cells, which differentially modulate NA release and processing in target networks (Devilbiss and Waterhouse 2011). Thus NA tone in LC-NA targets depends on LC-NA neuronal firing patterns, which in wakefulness are strongly modulated by hypocretin (Hcrt) (Walling et al. 2004). Among the wide range of afferents that project onto LC-NA cells, a prominent input indeed originates from the hypothalamic Hcrt neurons (Peyron et al. 1998; Horvath et al. 1999). Hcrt neurons also innervate all the other noradrenergic cell groups (A1, A2, A4, A5 and A7) in the hindbrain (Puskas et al. 2010). Hcrt was shown to increase LC neuronal firing rate in brain slices (Peyron et al. 1998; Cutler et al. 1999; Hagan et al. 1999; Horvath et al. 1999; Baldo et al. 2003; Puskas et al. 2010). RNA *in situ* hybridization for the two Hcrt receptors, *Hcrtr1* and *Hcrtr2*, revealed that the type 1 receptor is predominant in LC (Trivedi et al. 1998; Marcus et al. 2001; Darwinkel et al. 2014; Ch'ng and Lawrence 2015), but also abundant in the other pontine NA cell groups (A4, A5, and A7), while the nucleus of the solitary tract, which hosts the A2 NA cell group, shows lower *Hcrtr1* expression (Marcus et al. 2001)

Both optogenetic stimulation of Hcrt and LC-NA cells lead to an increase in the probability of state transitions from SWS or PS to wakefulness, however the awakening effect of LC-NA cell stimulation was found to display a considerably shorter delay than the one of Hcrt cell stimulation (Adamantidis et al. 2007; Carter et al. 2010). A photoinhibition of LC-NA cells concomitant with Hcrt neuron stimulation repressed Hcrt-mediated sleep-to-wake transitions, while co-stimulation enhanced awakening (Carter et al. 2012), indicating that the LC-NA cell group is an essential

effector in Hcrt-mediated arousal. Hcrt input to LC-NA has also been shown to be important in regulating wakefulness in the zebrafish (Singh et al. 2015).

Specific inactivation of Hcrtr1 signalling in NA targets remains unexplored. Here we created a mouse model with *Hcrtr1* gene inactivation in NA cells, by designing a conditional, Cre-dependent *Hcrtr1* allele (Vassalli et al. 2015), and crossing it with a Cre-expressing *Dopamine β-hydroxylase* (*Dbh*) PAC transgene (Parlato et al. 2007). The waking electrocorticogram of the resulting *Hcrtr1*$^{Dbh\text{-}cko}$ mice was examined in distinct behavioral paradigms. Relative to control littermates, spontaneous baseline wakefulness of *Hcrtr1*$^{Dbh\text{-}cko}$ mice demonstrated enhanced δ activity, suggestive of reduced alertness, while challenging behavioral contexts induced more profound spectral changes. Our study evidences the role of an intact Hcrt-to-NA signaling pathway to build an appropriate θ/fast–γ response in stress-associated environments, but also evidences circumstances in which the Hcrt-to-NA signaling pathway may serve to curb hyperarousal.

Results

Generating mice with NA cell-specific *Hcrtr1* deficiency. The *Hcrtr1* gene was engineered in embryonic stem cells to create a CRE-conditional *Hcrtr1* knockout (KO) (floxed, *Hcrtr1*^{flox}) allele (Fig. 1a). This allele is designed so as to be functional in absence of the CRE recombinase, while CRE mediates *loxP* site-recombination resulting in (i) deletion of the DNA encoding the signal peptide and N-terminal polypeptide up to within HCRTR1 transmembrane domain 3 (TM3) (126 aa in total), (ii) insertion of a promoter-less *Gfp* to report *Hcrtr1* promoter expression, and (iii) termination of transcription downstream of *Gfp* by insertion of a polyadenylation signal insuring effective *Hcrtr1* KO. To generate NA cell-specific HCRTR1 deficient mice, *Hcrtr1*^{flox} mice were crossed to transgenic mice expressing CRE from a *Dopamine-β-Hydroxylase* BAC transgene (*Tg(Dbh-Cre)*; Parlato et al., 2007). Breedings between *Hcrtr1*$^{flox/flox}$ mice where one parent is hemizygous for *Tg(Dbh-Cre)* produces two offspring groups, differing only in presence or absence of *Cre*: *Hcrtr1*$^{flox/flox}$ *Tg(Dbh-Cre)*$^{+}$ mice, in which NA-cells express *Cre* (hereafter referred as *Hcrtr1*$^{Dbh\text{-}CKO}$), and *Hcrtr1*$^{flox/flox}$ littermates, in which NA-cells do not express *Cre* (*Hcrtr1*$^{Dbh\text{-}CTR}$, or control mice). All analyses rely on pair-wise phenotype comparison between these two groups.

Moreover, a constitutive *Hcrtr1* KO allele (*Hcrtr1*$^{\Delta\text{-}GFP}$, Fig. 1a) spontaneously emerged in the colony through expression of *Tg(Dbh-Cre)* in the germ-line of a minority of *Hcrtr1*$^{Dbh\text{-}CKO}$ females, allowing us to generate a strain carrying the *Hcrtr1* loxP-recombined (KO) allele in all cells. This line expresses *Gfp* under control of the endogenous *Hcrtr1* promoter, permitting to map *Hcrtr1* expression in *Hcrtr1*$^{\Delta\text{-}GFP}$ heterozygote animals (Vassalli et al. 2015); Fig. 1d).

Validation of tissue-specific, Cre-dependent *Hcrtr1* gene recombination. Among seven brain NA cell groups, densest *Hcrtr1* expression is reported in the LC (Trivedi et al. 1998; Marcus et al. 2001; Darwinkel et al. 2014; Ch'ng and Lawrence 2015), thus our molecular and

histological analyses focused on this nucleus. To validate Cre-dependent *Hcrtr1*^{flox} recombination mutagenesis took place in the LC of *Hcrtr1*$^{Dbh\text{-}CKO}$ mice, genomic DNA was extracted from brain slices dissected to recover the LC area, cerebral cortex, and ear. Diagnostic PCR assays were designed to identify the *Hcrtr1*^{flox} allele, and the *Hcrtr1*$^{\Delta\text{-}Gfp}$ recombined allele. While cortex and ear DNA of both *Hcrtr1*$^{Dbh\text{-}CKO}$ and *Hcrtr1*$^{Dbh\text{-}CTR}$ mice could amplify only the *Hcrtr1*^{flox} products, DNA from the LC area of *Hcrtr1*$^{Dbh\text{-}CKO}$, but not *Hcrtr1*$^{Dbh\text{-}CTR}$ mice amplified both the *Hcrtr1*^{flox} and *Hcrtr1*$^{\Delta\text{-}Gfp}$ products. The latter band was gel-purified and DNA was sequenced from two 2 *Hcrtr1*$^{Dbh\text{-}CKO}$ animals, confirming at the nucleotide level correct recombination occurred, with inter-loxP DNA excision verified at both breakpoints.

GFP labeling of LC-NA cells in *Hcrtr1*$^{Dbh\text{-}CKO}$, but not *Hcrtr*$_1$ $^{Dbh\text{-}CTR}$ mice, evidencing deletion at the *Hcrtr1*^{flox} locus. To investigate the effect of Cre-mediated *Hcrtr1* locus recombination on gene expression in the LC, we used immunohistofluorescence imaging to assay CRE and GFP protein expression in LC-NA cells (Fig. 1b-h). Out of 732 TH-immunoreactive neurons in LC of *Hcrtr1*$^{Dbh\text{-}CKO}$ mice, 689 were positive for CRE immunostaining (94.3±2.1%, mean±SEM, n=3 mice; Figs 1e, g), and 96.8±1.4% of CRE-positive cells also expressed TH, confirming respectively penetrance and specificity of the *Dbh-Cre* transgene. Next, GFP immunostaining revealed bright GFP immunoreactivity in LC-NA cells of *Hcrtr1*$^{Dbh\text{-}CKO}$ mice (Fig. 1c), and its absence in *Hcrtr1*$^{Dbh\text{-}CTR}$ mice (Fig. 1b). Out of 674 TH-positive neurons in LC of *Hcrtr1*$^{Dbh\text{-}CKO}$ mice, 658 cells co-expressed GFP (97.6±1.3%, n=3 mice), while among 710 GFP-positive neurons, 92.9±2.4% co-expressed TH, indicating respectively efficiency and specificity of the Cre recombination having taken place at the *Hcrtr1*^{flox} locus. By comparison, in the LC of mice heterozygous for *Hcrtr1*$^{\Delta\text{-}GFP}$, in which all cells constitutively carry a recombined allele (Fig. 1a), out of 709 TH-expressing cells, 99.6±0.3% also expressed GFP (n=3 mice), and 91.2±4.6% of GFP-positive cells also expressed TH (Figs 1d, h). These data also confirm the robust activity of the *Hcrtr1* promoter in LC-NA cells.

Increased EcoG δ oscillatory power in baseline wakefulness of *Hcrtr1*$^{Dbh\text{-}CKO}$ mice. To assay electrocortical waking and ensuing sleep in various behavioral contexts, a cohort of *Hcrtr1*$^{Dbh\text{-}CKO}$ mice (n=9) and *Hcrtr1*$^{Dbh\text{-}CTR}$ littermates (n=7) were sequentially exposed to different experimental paradigms (Fig. 2). In the first two baseline days, time spent awake, in SWS and paradoxical sleep (PS) did not differ in the two groups (Fig. 3a and Suppl. Table 1). The ECoG spectral profiles in baseline wakefulness however differed (2-way ANOVA for genotype and frequency; genotype: $F_{1,\ 3822}$ =105.6; P<0.001; interaction between genotype and frequency: $F_{272,\ 3822}$ =1.5; P <0.001). In the first half of the dark phase (ZT12-18), *Hcrtr1*$^{Dbh\text{-}CKO}$ mice displayed higher ECoG power density in the δ frequency range (1.25 to 2.75 Hz) relative to control littermates (post-hoc t-test, P <0.05) (Fig. 3d). Both in humans and rodents, enhanced δ activity while awake is associated with drowsiness and reduced alertness, and progressively

increases as sleep pressure builds ups (Franken et al. 1991a); (Cajochen et al. 2002); (Lal and Craig 2002)). *Hcrtr1*$^{Dbh\text{-}CTR}$ mice' increase in δ power affected both the θ-dominated waking substate (TDW; Vassalli & Franken), and non-TDW waking (quiet wake), suggesting that *Hcrtr1*$^{Dbh\text{-}CKO}$ mice are globally less alert than controls.

Impaired electrocortical response to sleep deprivation (SD). A 6h period of enforced wakefulness through 'gentle handling' was initiated at light onset (ZT0) of the 3rd day, i.e. at a circadian time of maximal sleep propensity (Fig. 8a). In these 6h, relative to controls, *Hcrtr1*$^{Dbh\text{-}CKO}$ mice displayed increased activity across an extended range of low frequencies, compared to what had been observed in baseline (Fig. 3e, compared to d). Thus, EcoG power was enhanced across a wider δ range as well as in θ (0.75-8.0 Hz), and β (13.5-20.0 Hz) frequencies (independent two-tailed student's *t*-test, $P < 0.05$). A shift of ECoG power toward lower frequencies (over the δ, θ and α ranges) is known to correlate with decreased arousal (Cajochen et al. 1995; Aeschbach et al. 1997; Phipps-Nelson et al. 2011), while γ power wanes (Lal and Craig 2001; Lal and Craig 2002). When normalized to the baseline waking ECoG, SD was moreover found to induce a lesser increase in 8.75-9.5 Hz power in *Hcrtr1*$^{Dbh\text{-}CKO}$ mice than it did in controls, while a lesser decrease in inter-δ/θ band (4.5-7.0 Hz) activity is observed (Post-hoc independent two-tailed student's *t*-test, $P < 0.05$). This indicates that the θ rhythm acceleration, and θ peak sharpening, that normally occur in active waking in rodents, are blunted in *Hcrtr1*$^{Dbh\text{-}CKO}$ mice relative to their *Cre*-less littermates during SD.

Voluntary behaviors, both in threat-avoidance and appetitive arousal, correlate at the ECoG level, with the emergence of a high-power, narrow-bandwidth θ (~8-10 Hz) rhythm of hippocampal origin, as a stereotypical θ pattern becomes visible in the ECoG signal (Buzsaki, 2006). We have formulated an EEG-based algorithm to automatically score and quantify the behavioral state in which this pattern dominates (TDW, Vassalli & Franken, 2017). During SD, mice spend approximately 50% of their time in TDW (Vassalli & Franken, 2017). Hence we calculated the frequency of the θ rhythm in our mice during SD. *Hcrtr1*$^{Dbh\text{-}CKO}$ showed a significantly slower θ peak frequency (TPF) than controls (Fig. 3e; 8.1±0.1 Hz vs. 8.6±0.1 Hz, CKO vs. CTR; $t_{14} = -3.749$; $P=0.0022$). While in baseline, time spent in TDW state was unchanged in *Hcrtr1*$^{Dbh\text{-}CKO}$ mice relative to controls, during SD, *Hcrtr1*$^{Dbh\text{-}CKO}$ mice tended to express less TDW (Fig. 3b; 158.03±22.84 min (44%) vs. 203.23±18.81 min (56%), CKO vs. CTR; $P=0.165$). This tendency for reduced TDW state expression in SD is consistent with the impaired θ peak sharpening observed in these mice during SD.

Thus while SD induces the emergence of an ECoG θ synchrony in both genotypes compared to baseline waking (Fig. 1e compared to 1d), the frequency, and the synchrony, of this rhythm appear reduced in *Hcrtr1*$^{Dbh\text{-}CKO}$ mice relative to controls, suggesting that the hippocampal response to SD-associated arousal is blunted in *Hcrtr1*$^{Dbh\text{-}CKO}$ mice

Because TDW tends to correlate with enhanced locomotor activity (LMA), but can also uncouple

from it (Vassalli & Franken, 2017), as enhanced hippocampal θ can also be seen in immobile rats following running bouts (McFarland et al., 1975), or under motivational activation (Slawinska et al., 1998), we investigate LMA in our mice. LMA was found to be unchanged in the two baseline days, but to be markedly reduced during the 6h SD in *Hcrtr1*$^{Dbh\text{-}CKO}$ mice relative to control littermates (Fig. 3c; 929±120 vs. 1631±190 counts, in CKO vs. CTR; Fi; Mann-Whitney U test, P=0.01).

We next investigated the spectral dynamics of the waking ECoG in the course of the 3-day recordings (baseline BL1+BL2 days, 6h SD and recovery, see Fig. 2) in *Hcrtr1*$^{Dbh\text{-}CKO}$ and *Hcrtr1*$^{Dbh\text{-}CTR}$ littermates. Because waking spectra are strongly influenced not only by environmental contingencies, but also by homeostatic sleep pressure, waking ECoG power density values in the following analyses were referenced to the waking ECoG power density values in the last 4h of baseline light phase, i.e. when homeostatic sleep pressure is minimal, following the major sleep period.

Waking ECoG power dynamics during the 3-day recordings are depicted for each genotype in Fig. 4a, and differential CKO-CTR ECoG power dynamics are depicted in Fig. 4c (please note the different color coding of ECoG power in a vs. c). This analysis reveals a prominent deficit in *Hcrtr1*$^{Dbh\text{-}CKO}$ mice' θ rhythm regulation during the 6h SD (blue color-code), while δ and inter-δ/θ activities are markedly enhanced (orange/red color-codes), the latter in particular during the 2nd half of the SD, as sleep pressure builds up (Vyazovskiy and Tobler 2005). Another frequency range showing a deficit in power specifically during SD, in particular its 1st half, paralleling θ deficit, is the fast-γ (70-90 Hz) range.

Surprisingly, periods of high spontaneous activity (baseline dark phase waking maxima, Fig. 4b) were found to correlate, conversely, with enhanced θ/fast-γ activity in *Hcrtr1*$^{Dbh\text{-}CKO}$ mice relative to controls (Fig. 4c), an observation that will be confirmed in later recording days (see Fig. 6h), and be replicated during the nesting-associated wakefulness experimental paradigm (Fig. 5g).

Of note, maxima in ECoG power ratio time-courses (in heatmap spectral representations as depicted in Fig. 4a, or in dynamic analyses of ECoG power in specific frequency ranges normalized to their power in reference spectra, as depicted in Fig. 4d), do not represent maxima in brain oscillatory power, but the frequencies at which power densities maximally differ (see SFig. 1 for an illustration).

In sum, the full adaptive response of waking electrocortical parameters normally induced by the experimenter's 'gentle handling' manipulations appears impaired in *Hcrtr1*$^{Dbh\text{-}CKO}$ mice.

Altered electrocortical response to nesting-associated environmental enrichment, with θ/fast-γ responses inverse of those observed during SD. To explore the response of *Hcrtr1*$^{Dbh\text{-}CKO}$ mice to rewarding stimuli, rather than stress-associated stimuli such as SD, mice were exposed to a nest building experimental paradigm. Nest construction is an extremely robust, highly motivated behavior in mice ((Gaskill et al. 2013); (Eban-Rothschild et al. 2016)). Nest

material (a Nestlet™, see Methods) was introduced in the cage at dark onset (ZT12), and mice were left undisturbed across the night, up to light onset of the next day, at which time nest construction was assessed. All animals (CKO n=5; CTR n=5) had converted the Nestlet into an elaborated nest. Preliminary video-based behavioral analysis (in n=4/10 mice), indicated that most of nest-building activity took place in the end of the night phase, preceding the major sleep period. ECoG waking analysis thus focused on the last 6h (ZT18-24, Figs 5a, c), or last 2h (ZT22-24, Figs 5b, d), of the night. Providing nest material at the beginning of the night was found to markedly alter night phase wakefulness relative to SD-induced wakefulness, or to baseline waking. Surprisingly, wakefulness of *Hcrtr1*$^{Dbh\text{-}CKO}$ mutant mice was found to display enhanced fast-γ (50-80 Hz) power relative to controls in those time windows (Figs. 5a-b), in particular in the last 2h of the night, suggesting that Hcrt-to-NA signalling normally has a negative effect on fast-γ oscillations in this behavioral context.

Moreover, providing nest material to *Hcrtr1*$^{Dbh\text{-}CKO}$ mice induced enhanced waking β (15-30 Hz) and slow-γ (30.25-40.75 Hz) activities, relative to a night without such material, while this was not the case in *Hcrtr1*$^{Dbh\text{-}CTR}$ mice (Figs 5c-d). Elevated synchrony in the β and slow-γ ranges is observed in dopamine-depleted rodents and Parkinson disease patients, and found to correlate with motor dysfunction ((Lemaire et al. 2012);(Delaville et al. 2015)).

The spectral dynamics of wakefulness across the nesting night and the following 12h light phase were next examined. This confirmed the occurrence of prominent fast-γ power maxima (50-90 Hz) in *Hcrtr1*$^{Dbh\text{-}CKO}$ mice, which could be seen to occur mostly in the beginning and the end of the night in which nest material was available (Fig. 5g). Enhanced fast-γ activity was furthermore seen to correlate in its time-course with a θ rhythm enhancement. Enhanced θ rhythm and fast-γ power in *Hcrtr1*$^{Dbh\text{-}CKO}$ mice in the last 2h of the night (ZT22-24) furthermore correlated with a higher waking content (min/h) relative to control mice (Fig. 5f left), that might correlate with an increased nest-building activity. The following light phase also displayed three, shorter-lived, peaks of enhanced fast-γ activity, also temporally matched with peaks in θ rhythm.

The differential spectral dynamic analysis of wakefulness also confirmed *Hcrtr1*$^{Dbh\text{-}CKO}$ mice' enhanced slow-γ (30-50 Hz) activity compared to CTR in the nesting paradigm. Periods of higher slow-γ (30-50 Hz) power in CKO mice were seen to occur prominently in the first half of the night, and the first half of the following light phase.

Impaired electrocortical response to transfer from nesting cage to a new environment. After two intervening undisturbed days, mice were removed from their home cage where they had built their nest, and transferred to a fresh cage at ZT3, a time at which mice spontaneously mostly sleep (Fig. 8a). Cage change (CC) induces a powerful arising effect, and, although *Hcrtr1*$^{Dbh\text{-}CKO}$ mice tended to show reduced sleep latency following CC relative to control littermates (Fig. 6b), the two groups responded with a similar increase in time-spent-awake compared to their baseline values. The spectral quality of the waking ECoG was analyzed from CC

to SWS onset (see Methods), and found to significantly differ between genotypes (Fig. 6a top; two way ANOVA: genotype: $F_{1, 3276} = 40.360$; $P < 0.001$; interaction: $F_{272, 3276} = 1.822$; $P < 0.001$). The characteristic θ peak that defines active waking was apparent in both genotypes, but markedly blunted in *Hcrtr1*$^{Dbh\text{-}CKO}$ mice, which, similarly as observed during SD, displayed enhanced 3.25-6.25 Hz range activity, suggestive of reduced alertness. When CC-induced wakefulness was contrasted to wakefulness of the preceding 24h in the home cage (Fig. 6a bottom), and compared in the two genotypes (two way ANOVA: genotype: $F_{1, 3276} = 180.562$; $P < 0.001$; interaction: $F_{272, 3276} = 1.941$; $P < 0.001$), *Hcrtr1*$^{Dbh\text{-}CKO}$ mice displayed a lesser decrease in inter-δ/θ band activity than controls, again consistent with a partially failed narrowing, and acceleration, of θ oscillatory frequencies (see also Suppl. Table 2 for θ peak frequency values). Furthermore, the fast-γ response to CC across a wide frequency range (53-80 Hz) was profoundly diminished in *Hcrtr1*$^{Dbh\text{-}CKO}$ mice (Fig. 6a bottom; post-hoc independent two-tailed student *t*-test, $P < 0.05$). This effect is clearly apparent in heatmap representations of the waking ECoG spectral dynamics from CC to SWS-onset (Figs 6c-d). Thus, the fast-γ power response of *Hcrtr1*$^{Dbh\text{-}CKO}$ mice following CC is inversed relative to the one observed in these same mice, two days beforehand during the nesting night. This suggests that perception of the two behavioral contexts that are nesting in the dark phase, and forced exploration of a novel environment in the light phase, profoundly differ in their processing by the Hcrt-to-NA pathway, as further discussed below.

The heatmap representations of the spectral dynamics of CC-to-SWS wakefulness (Fig. 6c), and differential CKO-CTR dynamics thereof (Fig. 6d), also powerfully illustrate the blunted θ rhythm response of *Hcrtr1*$^{Dbh\text{-}CKO}$ mice to CC, compared to the *Hcrtr1*$^{Dbh\text{-}CTR}$ mice' response. Consistently with reduced θ synchrony in *Hcrtr1*$^{Dbh\text{-}CKO}$ mice, the decrease in inter-δ/θ band activity relative to its value at ZT8-12 of the preceding light phase, that is evident in controls (Fig. 6c right), is blunted in *Hcrtr1* mutant mice (Figs 6c left, and 6d).

We then performed a more specific dynamic analysis of ECoG power within specific frequency ranges. Based on their evident modulation in the course of the CC-to-SWS-onset waking paradigm as assessed in the heatmaps, three frequency ranges were analyzed (3.5-6.0 Hz (inter-δ/θ band), 7.5-11.5 Hz (θ), and 65.0-75.0 Hz(fast-γ); Fig. 6e). As time progresses after CC, novelty decreases and sleep pressure increases, the 3.6-6.0 Hz activity increased in both genotypes, while the θ and fast-γ activities decreased in both genotypes. At all time-points, however, and increasingly so at time progressed following CC, the 3.6-6.0 activity was higher in CKO than in CTR mice, while the θ and fast-γ activities were lower in CKO than in CTR littermates (independent two-tailed student's *t*-test, $P < 0.05$). In sum, although both *Hcrtr1*$^{Dbh\text{-}CKO}$ and *Hcrtr1*$^{Dbh\text{-}CTR}$ mice display a dramatic induction of θ synchrony, with a narrowing and acceleration of the θ rhythm, and of fast-γ oscillatory power, following CC (Fig. 6c), both these processes appeared significantly impaired in *Hcrtr1*$^{Dbh\text{-}CKO}$ mice (Fig. 6d).

To confirm that our unexpected observations of an opposite regulation of fast-γ oscillations in

waking of *Hcrtr1*$^{Dbh\text{-}CKO}$ mice in SD and after CC, on one hand (stress-associated stimuli), and in spontaneous and nesting-induced waking, on the other hand, was stable through time, we extended our spectral dynamic analysis of wakefulness throughout the day preceding CC, and the entire CC day. This revealed that spontaneous dark phase waking (in particular in ZT12-18) in the night preceding CC, and the night following CC, as had been observed for baseline recording days 1 and 2, witness a concerted surge in θ and fast-γ power, present in both genotypes, but *enhanced* in *Hcrtr1*$^{Dbh\text{-}CKO}$ animals (Fig. 6f-h).

Slow-wave-sleep of *Hcrtr1*$^{Dbh\text{-}CKO}$ mice, in particular following active waking, is markedly deficient in the slow-δ oscillatory component. Because SWS quality critically depends on preceding wakefulness quality, in particular on prior time animals spent in the TDW waking substate (Vassalli & Franken, in revision), we next examined SWS subsequent to the distinct behavioral contexts the mice were exposed to. We thus analyzed the mice' global baseline (48h) SWS spectral profiles (Fig. 7a), the profiles of the first 20 min of SWS following baseline light-onset (Fig. 7c), i.e. when sleep homeostatic drive is maximal, after the mice' major waking period (Fig. 3a), the first 20 min of SWS following SD (Fig. 7b), and following CC-induced waking (Fig. 7d). A slow (~0.75-2.00 Hz) and fast (~2.50-4.25 Hz) ranges of δ power were seen to respond differently in *Hcrtr1*$^{Dbh\text{-}CKO}$ mice, with a more pronounced deficiency in slow-δ than in fast-δ power, respective to controls. While this deficit was visible but below significance in baseline, it became more pronounced in post-SD and post-CC SWS, suggesting that SWS subsequent to stress-associated active waking is more dependent on Hcrt-to-NA signalling than baseline waking is. In SWS following nesting-induced waking we did not observe a δ, or selective slow-δ, power deficit (not shown). Post-SD SWS of *Hcrtr1*$^{Dbh\text{-}CKO}$ mice moreover displayed enriched β and slow-γ activities (Fig. 7b). Increased β power during non-REM sleep is reported in insomnia in humans (Spiegelhalder et al., 2012).

SWS spectra of *Hcrtr1*$^{Dbh\text{-}CKO}$ mice in these distinct experimental contexts were next plotted in reference to the spectra of control littermates in the same contexts (Fig. 7e). The resulting CKO/CTR ECoG power ratio spectral distribution confirms that the major genotype differences in SWS quality reside in the slow-δ band. Moreover, the altered spectral responses of CKO mice' SWS relative to CTR mice' SWS were seen to closely overlap, and be more pronounced in post-SD and post-CC SWS, than they were in baseline SWS, emphasizing again that SD and CC similarly affect electrocortical activity across behavioral states, and similarly rely on Hcrt-to-NA signalling.

Time-course analyses of SWS slow-δ and fast-δ power (Fig. 8b) across the 3-day recording revealed that at all time points slow-δ power is dimished in *Hcrtr1*$^{Dbh\text{-}CKO}$ mice relative to controls, however this deficit is enhanced following major waking periods (at the end of the night, and after SD, Fig. 8b; and after CC-induced waking (Fig. 8d).

The significance of different δ oscillatory frequency ranges in SWS, and their potential impact on homeostatic recovery, remain unclear. However, a correlation of the slow-δ component of SWS

with prior active wakefulness, TDW and potentiation events was reported in several studies, including by ourselves in *Hcrt-KO* mice (Vassalli & Franken), and is further discussed below. Our present data suggest that events associated with active waking critically require Hcrt-to-NA signalling for subsequent SWS expression of a slow-δ oscillatory component.

Discussion

Here we record brain activity in a novel mouse line engineered to carry a non-functional *Hcrtr1* gene in NA cells, in four distinct behavioral contexts (spontaneous baseline waking, gentle handling-enforced waking, nesting-associated, and CC-induced waking), and follow their electrocortical and behavioral state response. Relative to control littermates, the spectral oscillatory profile of *Hcrtr1*$^{Dbh\text{-}CKO}$ mice' wakefulness is more extensively altered as mice are placed under behavioral challenge. Moreover the electrocortical alterations are found to be highly context-dependent, with, in particular, an opposite regulation of fast-γ oscillations in distinct contexts. Because these changes were robust and reproducible, we suggest they may eventually inform on novel aspects of noradrenergic regulation of behaviors and affects.

The TDW waking substate (Vassalli & Franken) (or 'active waking') is characterized at the ECoG level by a narrowing and frequency increase of the θ oscillatory peak, and enhanced fast-γ activity, as the mouse gets aroused. Our most salient finding is that the induction of these two read-out's of arousal is markedly diminished in *Hcrtr1*$^{Dbh\text{-}CKO}$ mice relative to control littermates in SD and following CC, whereas in spontaneous dark phase and nesting-associated wakefulness, the θ and fast-γ oscillatory responses now show an inverse relation to controls, i.e. show marked enhancement in *Hcrtr1*$^{Dbh\text{-}CKO}$ mice.

Terminology. Waking in rodents is often partitioned in two broad substates, quiet and active waking (McGinley et al. 2015). In quiet waking and automatic behaviors, activity distributed across the 4.0-7.0 Hz range is known to increase with sleep drive, and perception of sleepiness ((Franken et al. 1991a; Vyazovskiy and Tobler 2005)and see below. Although it is commonly referred to as 'θ', we here refer to it as the 'inter-δ/θ' frequency range, to distinguish it from the hippocampally-driven θ rhythm of active wakefulness (Buzsaki 2002). In voluntary behaviors, such as in explorative locomotion, foraging, but also in alert immobility, a higher-frequency (7-10 Hz), narrow-bandwidth θ rhythm of hippocampal origin appears, as the raw EEG signal displays a regular, stereotypical rhythmic pattern (McFarland et al. 1975; Slawinska and Kasicki 1998), that we designed an algorithm to recognize, and define as the TDW substate (Vassalli & Franken).

Altogether, relative to *Hcrtr1*$^{Dbh\text{-}CTR}$ littermates, *Hcrtr1*$^{Dbh\text{-}CKO}$ mice' wakefulness manifested:
(i) a slowing of the electrocorticogram, with enhanced power in the δ and inter-δ/θ ranges,
(ii) enhanced β and slow-γ activity, particularly pronounced in nesting-associated-waking,
(iii) impaired θ rhythm induction under SD and following CC.

(iv) impaired θ rhythm induction following CC is correlated with impaired fast-γ power induction.
(v) Conversely, fast-γ power is enhanced in spontaneous dark phase and nesting behaviors.

Hcrt-to-NA signalling deficiency causes a slowing of the ECoG in stress-associated contexts (SD and CC). Baseline waking of *Hcrtr1*$^{Dbh\text{-}CKO}$ mice shows enhanced power in a restricted, slow-δ (1.25-2.75 Hz), range, while SD, nest material provision and CC induce ECoG alterations over the entire spectral range, encompassing the δ, inter–δ/γ, β, slow- and fast-γ ranges. SD and CC induce enhanced δ and inter-δ/θ activities, both of which are reported to be markers of homeostatic sleep pressure in the waking ECoG of rodents and humans (Franken et al. 1991b; Cajochen et al. 1995; Finelli et al. 2000; Huber et al. 2000; Vyazovskiy & Tobler 2005), and to correlate with subjective experience of sleepiness in humans (Lal and Craig 2002). In humans, a gradual increase in waking δ activity is paralleled by decrements in cognitive performance (Dijk et al. 1992). While slow frequencies show enhanced activity in *Hcrtr1*$^{Dbh\text{-}CKO}$ mice following CC, fast-γ is reduced. Slowing of the ECoG suggests reduced alertness of *Hcrtr1*$^{Dbh\text{-}CKO}$ mice in SD and CC.

Enhanced β and slow-γ activity. Nesting-associated waking was enriched in β (15-30 Hz) and slow-γ (30.25-40.75 Hz) power in *Hcrtr1*$^{Dbh\text{-}CKO}$ mice. Pathological β oscillations are present in Parkinson's disease patients as an 'anti-kinetic rhythm', correlated with motor dysfunction and responding to treatment (Hammond et al. 2007; Engel and Fries 2010; Jenkinson and Brown 2011) Enhanced β and slow-γ activity is also seen in dopamine-depleted rodent models, and is particularly pronounced when mice perform particular tasks (Lemaire et al. 2012; Delaville et al. 2015) Whether enhanced β and slow-γ activity in *Hcrtr1*$^{Dbh\text{-}CKO}$ mice reflects dopaminergic deregulation is unknown, but its association with a motor impairment can be tested in our mice, and is supported by the fact that *Hcrt*-KO mice also show enhanced slow-γ (30-47.5 Hz) activity in wakefulness of the minute that precedes cataplexy attacks (Vassalli et al. 2013). The latter are most often triggered during motivated behaviors including nest-building, and the postural collapse that characterizes them is sometimes preceded by evident impaired motor control, such as leg stumbling, thought to represent partial cataplexies.

Impaired θ rhythm induction. The θ rhythm modulation we observe in *Hcrtr1*$^{Dbh\text{-}CKO}$ mice are aligned with many studies demonstrating the role of LC-NA activation in promoting hippocampal, and neocortical θ oscillations (Berridge and Foote 1991); (Walling et al. 2011); (Vazey and Aston-Jones 2014). Our study suggests that some of these effects critically rely on Hcrt input.

Our observation of impaired θ rhythm induction, but enhanced β/slow-γ activity, in *Hcrtr1*$^{Dbh\text{-}CKO}$ mice during SD corroborate a rat study in which stimulation of the LC was found to enhance θ activity, but suppress 12 to 40 Hz frequencies, through a pathway involving inhibition of a type of

dentate gyrus interneurons (Brown et al. 2005). Presynaptic Hcrtr1 signaling in hippocampal noradrenergic terminals may thus be implicated in the behaving animal in θ and slow-γ regulation.

Inversed θ/fast-γ responses of *Hcrtr1*$^{Dbh\text{-}CKO}$ mice in SD and CC vs. spontaneous dark phase and nesting-associated waking. Relative to controls, *Hcrtr1*$^{Dbh\text{-}CKO}$ mice display lower fast-γ activity during SD and post-CC wakefulness, while spontaneous dark phase waking, and increasingly so dark phase waking in presence of nest material, display higher fast-γ power. What could explain these opposite θ/fast-γ responses in distinct behavioral contexts?

Hcrtr1 signalling has been implicated in fear and fear memory, in particular for memories with a high emotional component (Soya et al. 2013); (Flores et al. 2014). *Hcrtr1*-KO mice display a reduced freezing time in cue-dependent fear memory tests, which could be restored by AAV-mediated expression of *Hcrtr1* in LC-NA cells (Soya et al. 2013) After the acquisition of fear memory, Hcrtr1 blockade was shown to facilitate fear extinction and decrease freezing time (Flores et al, 2014). Notably, intra-amygdala infusion of Hcrtr1 antagonists enhanced fear extinction, suggesting that noradrenergic axons within the amygdala arising from the LC express Hcrtr1, and that presynaptic Hcrtr1 signalling enhances the fear response (Flores et al, 2014).

One working hypothesis therefore would be that loss of Hcrtr1 expression in LC-NA cells causes blunting of the fear response, and of the θ/fast-γ oscillatory activation associated with frightened arousal, upon human manipulation (during SD), or exposure to a foreign environment (after CC), reflected in the electrocorticogram with failed θ and fast-γ responses.

In contrast, in spontaneous dark phase and nesting behaviors, the θ rhythm and fast-γ responses may be mediated by other pathways, that are preserved in *Hcrtr1*$^{Dbh\text{-}CKO}$ mice. Because nesting and spontaneous dark phase behaviors are rewarding (Gaskill et al. 2013), induce arousal, the TDW state, and associated θ/fast-γ oscillatory activation, a reduced fear response may permit expression of enhanced behavioral activation during nest-building, reflected in the enhanced θ and fast-γ response of *Hcrtr1*$^{Dbh\text{-}CKO}$ mice in the two latter contexts. Supporting this argument, hippocampal θ is induced not only by locomotion, but also by motivational activation (Slawinska and Kasicki 1998). This raises the interesting possibility that an enhanced level of θ/fast-γ oscillatory activation in *Hcrtr1*$^{Dbh\text{-}CKO}$ mice may, in some circumstances, lead to hyperarousal.

Hcrt-to-NA signalling deficiency did not cause overt cataplexy. *Hcrtr1*$^{Dbh\text{-}CKO}$ mice did not demonstrate obvious electrocortical, or behavioral, evidence of cataplexy (Chemelli et al. 1999); (Vassalli et al. 2013). A strong body of evidence in the canine model of narcolepsy implicated the NA system in the control of cataplexy (Nishino and Mignot 1997), leading to the noradrenergic hypoactivity hypothesis. Although a more thorough, video-based, behavioral assessment of our mice is warranted, our preliminary observation is in concordance with the finding that restoration of *Hcrtr1* in LC of mice lacking Hcrt receptors did not suppress cataplexy (Hasegawa et al. 2014). Also, genetic canine models of narcolepsy are caused by loss-of-function mutations in *Hcrtr2* and

not *Hcrtr1* (Lin et al. 1999). One explanation may be that, an yet unknown Hcrtr2-expressing cell population critically controls LC-NA neurons and cataplexy.

A limitation of the present work is that Hcrtr1-mediated signalling is inactivated in our mice as soon as *Dbh* is expressed, i.e. around mid-embryonic development (Cre-mediated activity was first evidenced in *Tg(Dbh-Cre)* mice at E11.5; (Parlato et al. 2007). Thus the effects we observe may differ, and may be milder, from those of acute NA cell-specific Hcrtr1 inactivation. Exploring the latter is feasible in our mice through local viral transduction of a NA cell-specific Cre-expressing vector in the LC, or another NA cell group that express *Hcrtr1*, in adult *Hcrtr1*$^{flox/flox}$ mice.

Hcrt-to-NA signalling deficiency affects the spectral quality of SWS. How does Hcrt-to-NA signalling relate to wake/sleep homeostatic processes? Our work revealed that this pathway is essential during waking in stressful conditions for normal expression of slow-δ oscillations in ensuing sleep.

A selective deficit in slow-δ is also seen in SWS of *Hcrt*$^{ko/ko}$ mice following spontaneous baseline waking (Vassalli & Franken), as well as in SWS of rats following SD if they were depleted in cortical NA (Cirelli et al. 2005). These rats furthermore display reduced cortical expression of synaptic activity-associated genes during SD waking (Cirelli et al. 2004), as do Hcrt-KO mice in spontaneous baseline dark phase (Vassalli & Franken). The significance for sleep recovery function of a specific slow-δ deficit in SWS, is unclear, but the above studies suggest that slow-δ power in SWS is dependent upon NA-dependent, and possibly Hcrt-dependent, potentiation events in preceding wakefulness. Because θ activity is known to be associated with heightened synaptic plasticity and memory-related potentiation events, and long-term potentiation (LTP) in the hippocampus is optimally induced by θ frequency stimulation (Larson et al. 1986), reduced θ promotion under SD and CC in *Hcrtr1*$^{Dbh\text{-}CKO}$ mice may also cause a deficit in hippocampal potentiation events, and thus affect learning and memory.

We previously found that time spent in TDW state is a predictor of sleep homeostatic drive, as δ power in ensuing SWS is correlated with prior time spent in TDW, rather than in all waking (Vassalli & Franken). *Hcrt*-deficient mice, which are profoundly impaired in maintaining TDW in baseline conditions, express a subsequent SWS markedly diminished in δ power, in particular in the slow-δ range (Vassalli & Franken, 2017). Thus impaired slow-δ in SWS of *Hcrtr1*$^{Dbh\text{-}CKO}$ mice following SD, may be related to their deficit in θ rhythm sharpening and frequency during SD. Supporting this, TDW state expression tends to be reduced in *Hcrtr1*$^{Dbh\text{-}CKO}$ mice during SD, although this variable failed statistical testing in our mouse sample.

Using simple electrocortical indices of the waking state and SWS quality, we here provide suggestive evidence of the functional relevance of the Hcrt-to-NA connection in adaptive regulation of behaviors amid changing contexts. We expect many behaviors to be affected by the

loss of noradrenergic Hcrtr1 signalling in our mutant mice. Deciphering the underlying mechanisms, and potential therapeutic use of Hcrt receptor and noradrenergic pharmacological agents, will particularly benefit from a better understanding of how Hcrt neuronal firing patterns affect LC-NA cell firing patterns, and the identification of the sites at which Hcrtr1 signalling mediates its behavioral affects.

Methods

***Hcrtr1* mutagenesis: generation of the *Hcrtr1^{flox}* allele.** A floxed allele of the mouse *Hcrtr1* gene (*Hcrtr1$^{tm1.1Ava}$* MGI: 5637400) (hereafter referred to as *Hcrtr1^{flox}*) was created. The *Hcrtr1^{flox}* allele was designed to be functional in absence of CRE and to undergo *loxP* site- specific recombination in presence of CRE, resulting in deletion of the coding region for HCRTR1 signal peptide and N-terminal polypeptide up to within TM3 (deletion of 126 aa in total). Furthermore, the 5' coding sequence of the receptor is replaced by a *Gfp* coding sequence, followed by a polyadenylation signal, thus most likely resulting in transcript termination. Cre-mediated *loxP-loxP* DNA excision thus places *Gfp* into the first coding exon, and leads, in recombined cells, to its expression in place of *HcrtR1*, under the control of the endogenous *Hcrtr1* promoter. Targeting design: The *5'loxP* site was inserted in the 5' untranslated region of *Hcrtr1'* first coding exon (Exon 3, Chen and Randeva, 2004), 27 bp downstream of Exon 3 splice acceptor site and 12 bp upstream of the initiation codon, by replacement of an AccI-ApaI fragment. The 3' loxP site was inserted midway in Intron 4 as a *loxP-Kozak-GFP-rabbit globin p(A)-FRT-Neo-FRT* cassette. To introduce these mutations at the *Hcrtr1* locus, a targeting vector was constructed using PAC RP23-12J1 (chromosome 4) as PCR template. Two homology arms (spanning in total 10.0 kb of the *Hcrtr1* locus) were generated using the PAC template and LA Taq polymerase (Takara) and Accuprime High-Fidelity Polymerase (invitrogen). The targeting vector was linearized and electroporated in IC1 embryonic stem cells (*C57BL/6NTac*, ingenious targeting laboratory, Ronkonkoma, NY, USA) and two ES cell clones having undergone correct recombination events were identified by Southern blotting, and injected into *BALB/cAnNHsd* blastocysts. To excise the FRT-neo-FRT cassette, resulting chimeras were crossed to *Tg(ACTFLPe)9205Dym* transgenic mice.

Generation of NA cell-specific *Hcrtr1*-KO mice. To inactivate *Hcrtr1* in NA cells, mice harboring the *Tg(Dbh-icre)^{1Gsc}* transgene, derived from a PAC harboring the *Dopamine-β-hydroxylase* gene (*Dbh*) (Parlato et al., 2007), were mated to *Hcrtr1^{flox}* mice. Phenotype analysis is based upon paired-wise comparison between *Hcrtr1$^{flox/flox}$ Tg(DBH-Cre* hemizygous mice (hereafter referred to as *Hcrtr1$^{DBH\text{-}CKO}$*, CKO), and *Hcrtr1$^{flox/flox}$* littermates (lacking the Cre-expressing transgene) (referred to as *Hcrtr1$^{DBH\text{-}CTR}$*, CTR). All mice share a *C57BL/6NTac x C57BL/6J* mixed genetic background.

Evidence of tissue-specific, Cre-dependent *Hcrtr1^{flox}* allele recombination. We designed 2 PCR assays flanking *Hcrtr1^{flox}* loxP sites, allowing amplification of a diagnostic fragment from the recombined allele, and a 1.1 kb larger fragment (inter-loxP distance) from the non-recombined allele. The corresponding recombined fragments were produced from DNA prepared from tissue slices containing the LC (250 um X 1mm X 1mm tissue piece) from *Hcrtr1$^{Dbh\text{-}CKO}$* animals, but not from *Hcrtr1$^{Dbh\text{-}CTR}$* littermates, or not from their ear DNA. PCR products were gel purified and the

loxP recombined junction was sequenced in both orientations, allowing to confirm accurate recombination at the nucleotide level in 2 *Hcrtr1*$^{Dbh\text{-}CKO}$ animals.

Generation of the *Hcrtr1* KO/GFP reporter (*Hcrtr1*$^{\Delta\text{-}Gfp}$) allele. Spontaneous expression of *Tg(Dbh-Cre)* in the germ-line was found to occur in a minority of *Hcrtr1*$^{flox/flox}$ +/*Tg(Dbh-Cre)* females, allowing us to generate a line carrying the recombined allele derived from *Hcrtr1*$^{tm1.1Ava}$ in the germ-line (*Hcrtr1*$^{\Delta\text{-}GFP}$, or *Hcrtr1*$^{tm1.2Ava}$ MGI: 5637400). Accuracy of the loxP site recombination at the *Hcrtr1*$^{\Delta\text{-}Gfp}$ allele was verified by sequencing of genomic DNA from ear biopsies of 2 male mice homozygous for the mutation.

Mice. All ECoG data are derived from 10-13 week-old males (weight 27-31 g). Mice were individually housed with food and water *ad libitum* under a 12h light/12h dark cycle (lights on at 8:00 am, defined as *Zeitgeber* Zero, ZT0). All experiments were performed in accordance with Swiss federal legislation, using protocols approved by the State of Vaud Veterinary Office, Switzerland.

ECoG/EMG, video and locomotor activity (LMA) recording. Electrodes for differential fronto-parietal EEG and EMG recording were implanted as described (Mang and Franken 2012). Hardware (EMBLA A-10) and software (Somnologica-3) were from Medcare Flaga (EMBLA, Thornton, USA). EEG and EMG signals were amplified, filtered, analog-to-digital converted, and stored at 200 Hz. Each 4-s epoch was assigned a behavioral state score using published criteria (Franken et al. 1998). Behavioral monitoring was performed using infrared video-cameras allowing close frontal viewing. Locomotor activity was assessed at 1-min resolution using top-mounted passive infrared motion detectors (Visonic Ltd, Tel Aviv, Israel) and analyzed with ClockLab software (ActiMetrics, IL, USA).

ECoG power spectral density analysis. The ECoG signal was subjected to discrete Fourier transform to yield power density spectra (0.75–90 Hz) in 4s consecutive epochs (0.25 Hz frequency resolution; Hamming window function). Values between 47.5 to 52.5 Hz were excluded because of the 50 Hz AC power line noise. Higher-frequency artefacts (e.g. 71.25-77.25 Hz) of unknown origin were present in some mice (SD: 6/16; 3 CKO, 3 CTR; CC: 4/14; 1 CKO, 3 CTR; Nest experiment: 4/10; 1 CKO; 3 CTR), and values in these frequency ranges were removed from spectral analysis. Artefacted epochs were tagged and removed from spectral analysis but not from time-spent–awake/-in-SWS, when behavioral state could be assessed. For each behavioral state and animal, a mean ECoG spectrum was obtained by averaging the spectra of all epochs that were artefact-free and flanked by the same state (Franken et al. 1998). To account for inter-individual differences in overall ECoG power, ECoG spectra of were expressed as a percentage of an individual reference value calculated as the total ECoG power across frequencies (0.75-40 Hz)

and behavioral states. This reference was weighted so the relative contribution of each state is identical in all animals (Franken et al. 1998). Reference values for the two genotype did not differ (*Hcrtr1*$^{Dbh\text{-}CKO}$ *vs.* *Hcrtr1*$^{Dbh\text{-}CTR}$ 1181± 127 uV^2 *vs.* 1181± 120 uV^2, t_{14}= 0.00105, *P*=0.99). The dominant frequency of θ oscillations (θ peak frequency, TPF) was determined for each animal as the frequency at which ECoG power density of the mean spectral profile was highest in the 5-10 Hz range during waking (Hasan et al. 2009; Mang et al. 2016).

Behavioral exposure. Cohorts of *Hcrtr1*$^{Dbh\text{-}CKO}$ and *Hcrtr1*$^{Dbh\text{-}CTR}$ (n=9:7, CKO:CTR) littermate mice were sequentially exposed to four experimental contexts, as their ECoG/EMG data were acquired: (i) baseline (undisturbed) conditions, (ii) SD, (iii) nest-building, (iv) transfer to fresh cage. Only uninterrupted high-quality recordings with appropriate experimental set-up were considered for analysis. Hence, (i-ii): n=9:7; iii: n=5:5; (iv):n=8:6 (CKO:CTR) animals were analyzed.

Baseline and sleep deprivation (SD)-induced wakefulness: '3-day recordings' consisted of two undisturbed days (BL1+BL2), followed by a 6h SD initiated at light onset (ZT0) of the 3rd day. SD was achieved by 'gentle handling' (Mang and Franken 2012). To further stimulate behavioral activity during SD, tissue paper was introduced in homecage at ZT2 and ZT5, and midway through SD (ZT3), mice were transferred into a fresh cage. Following SD, mice were left undisturbed for the rest of the day, and for at least another 2 intervening days.

Nest material interaction experiment: Nest material previously shown to trigger cataplexy in Hcrt-deficient mice (Vassalli et al. 2013) was used, i.e. Nestlets^{TM} (Ancare, Ref. Nr. 14010), made of highly shreddable cotton. One Nestlet was introduced in the cage at dark onset (ZT12) of day 6, and mice were left undisturbed until next light-onset and nest-building assessment. Mice were then left undisturbed for another ≥2 more days before the next experiment.

Cage change (CC): On ZT3 of day 9, mice were transferred from their homecage where the nest had been built to a fresh cage. Latency to SWS onset was defined as the time until the first SWS episode lasting ≥2 min and interrupted by ≤3 epochs scored as wakefulness (Hunsley et al. 2006).

Brain immunohistofluorescence. ~16-wk old mice were deeply anesthetized with sodium pentobarbital (100 mg/kg, i.p), perfused with 4% paraformaldehyde, pH 7.4. Brains were quickly removed, post-fixed in the same fixative for 2h at 4°C, immersed successively in 15% (1h), and 30% sucrose (o/n) at 4°C, frozen and stored at -80°C until use. Coronal sections (20-μm) were collected on SuperFrost-Plus glass slides, blocked in 2% BSA, 5% normal donkey serum, 0.3% TritonX-100 in 1xTBS (pH 7.5) for 30min at r.t., and antibodies applied in 1xTBS, 1% BSA , 0.2% TritonX-100, and incubated o/n at 4°C. Antibodies were: tyrosine hydroxylase (TH) from mouse (Incstar, Cat. 22941; 1:5000), green fluorescent protein (GFP) from chicken (Aves Labs, Cat.

1020; 1:500), and Cre recombinase (Cre) from rabbit (Novagen, Cat. 69050-3; 1:500). Secondary antibodies were donkey IgGs coupled to Alexa dyes used at 1:500 for 1h at r.t. Images were acquired on an inverted Zeiss LSM710 confocal laser-scanning microscope using ZEN, and analyzed using ImageJ.

Statistics. Data were tested for normal distribution using Shapiro-Wilk normality test. If the test passed, genotype differences in TPF and accumulated LMA during SD, or ECoG power within specific frequency bands were evaluated by independent two-tailed student's *t*-test. Otherwise, nonparametric Mann-Whitney test was used. Time-course of hourly values of W, SWS, PS, LMA, ECoG power spectra, were analyzed by two-way ANOVA with factors "genotype" and "time-of-day", or "genotype" and "frequency bin", and their interaction. When significance was reached for the main factors and/or their interactions, genotype contrasts were assessed by unpaired, two-tailed Student's *t* tests. Within-group effects, such as response to SD or nest material, were assessed using paired, two-tailed student's *t*-tests. $P<0.05$ was considered as significant, and results are reported as mean±SEM. TMT Pascal Multi-Target5 software (Framework Computers, Inc., Brighton, MA, USA) was used to process data, and SPSS V23 (IBM SPSS Statistics, Armonk, NY, USA) or SAS V9.2 (SAS Institute Software Inc., Cary, NC, USA) for statistical analysis. Figures were prepared using SigmaPlot V12.5 (Systat Software Inc., Chicago, IL, USA) and Adobe Illustrator CC 2015 (Adobe Systems).

Figure Legends

Fig. 1. Targeted mutagenesis at the *Hcrtr1* locus. (**a**) Homologous recombination between our *Hcrtr1* targeting vector (see Methods) and the *Hcrtr1* gene generated a functional, but Cre-dependent KO, *Hcrtr1* allele (*Hcrtr1*^{flox}). In *Hcrtr1*$^{flox/flox}$ mice hemizygous for *Tg(Dbh-Cre)* (Parlato et al., 2007), Cre expression in noradrenergic cells results in loxP site-specific recombination, inter-loxP genomic deletion, producing the *Hcrtr1*$^{\Delta\text{-}GFP}$ allele, with deletion of a 126 aa-encoding region of *Hcrtr1*, and, in cells expressing the *Hcrtr1* promoter, *Gfp* expression and transcript termination. Ex, exon; FRT, flippase recognition target; pA, polyadenylation site; TSS, transcription start site. Adapted from Vassalli et al., *Sci Transl Med.* 2015 Nov 18;7(314):314le2. (**b-h**) Immunohistofluorescence validation of the specificity and efficiency of Cre-mediated recombination at the *Hcrtr1*^{flox} allele. Representative photomicrographs depicting (**c**) TH (red) colocalizing with GFP (green) in LC of an *Hcrtr1*$^{Dbh\text{-}CKO}$ (CKO) mouse, and (**d**) in LC of an *Hcrtr*$_1$$^{+/\Delta\text{-}GFP}$ mouse with whole-body deletion in *Hcrtr1*, but (**b**) absence of GFP immunostaining in LC of a *Hcrtr1*$^{Dbh\text{-}CTR}$ (CTR) mouse. (**e**) TH colocalizes with CRE (green) in LC of an *Hcrtr1*$^{Dbh\text{-}CKO}$ mouse. (**f-h**) Quantification of TH co-expression with GFP or CRE in brain sections collected at 4 coronal levels from rostral to caudal LC (Bregma: -5.34 to -5.68 mm). Absolute cell count per 20-μm section are shown (mean±SEM, n=3 CKO, and n=3 *Hcrtr*$_1$$^{+/\Delta\text{-}GFP}$ mice). 4V, 4th ventricle. *Dbh*, *Dopamine-β-hydroxylase* gene promoter; TH, Tyrosine hydroxylase. Scale bars: 100 μm for low magnification; 50 μm for high magnification. Mouse Genome Informatics **www.informatics.jax.org/reference/j:226158**: *Hcrtr1*^{flox} is *Hcrtr1*$^{tm1.1Ava}$ (MGI:5637400); *Hcrtr1*$^{\Delta\text{-}GFP}$ is *Hcrtr1*$^{tm1.2Ava}$ (MGI: 5637401).

Fig. 2. Experimental design. The same cohort of mice (*Hcrtr1*$^{Dbh\text{-}CKO}$, n=9; *Hcrtr1*$^{Dbh\text{-}CTR}$, n=7) were sequentially exposed to distinct behavioral paradigms. Spontaneous waking ECoG is analyzed in two baseline (undisturbed) days, followed by a 6h 'gentle handling' sleep deprivation (SD), initiated at light onset (ZT0) of the 3rd day. After 2 intervening days, nest material (+Nestlet) is introduced at dark onset (ZT12), and the waking ECoG analyzed in the following 24h. After an additional 2 intervening days, the mouse is removed from its nesting cage, and transferred to a fresh cage 3h after light onset (ZT3). Post-CC waking is analyzed until the next SWS onset (see Methods). Shaded areas represent the 12h dark phases.

Fig. 3. Spontaneous vs. enforced wakefulness. Time-courses of (**a**) wakefulness [min/h], (**b**) θ-dominated-wakefulness (TDW) [min/h], and (**c**) locomotor activity (LMA) [counts/h] (mean±SEM) in the first three days of recording. (**d-e**) ECoG power density spectra of wakefulness (W) in the first half of the baseline dark phase (ZT12-18) (**d**), or the 6h SD (**e**) for *Hcrtr1*$^{Dbh\text{-}CKO}$ mice (CKO, black) and *Hcrtr1*$^{Dbh\text{-}CTR}$ (CTR, grey) littermates. Power density values [%]

are referenced to each mouse' total ECoG power across all states and frequencies in baseline (Franken et al. 1998). Note non-linear axes. Blown-up views across 0.75 to 15 Hz (**d**), and 6.5 to 10 Hz (**e**), with linear axes, are shown in insets. Baseline dark phase waking shows enhanced δ-range activity in CKO mice relative to CTR, while SD-waking shows an extended range of power increase, over δ, inter-δ/θ band and β-range activities. SD-waking displays a slowing of the θ rhythm in CKO relative to CTR mice (**e** inset). θ peak frequency (TPF) value (mean±SEM) is shown for CKO (black symbol) and CTR (grey) mice. Red bars and asterisk indicate significant genotype differences (two-way ANOVA, followed by post-hoc independent two-tailed student *t*-test, $P<0.05$).

Fig. 4. Gentle handling-induced SD waking of *Hcrtr1*$^{Dbh\text{-}CKO}$ mice displays blunting of the θ rhythm and fast-γ activity responses relative to controls. (**a**) Heatmap representation of the waking ECoG spectral dynamics across the 3-day BL1-BL2-SD recording. Waking ECoG power in each 0.25 Hz frequency bin was calculated across time relative to each mouse' mean ECoG power in that frequency bin in wakefulness of baseline (BL1-BL2) light phase last 4h (ZT8-12) (plotted as $\log_2$ value, and color-coded as shown on the right). (**b**) Waking time-courses [min/h] are plotted below. (**c**) Differential (CKO-CTR) heatmap dynamics of the waking ECoG in the 3-day recording. To emphasize genotype differences, the two spectral dynamics shown in (**a)** were substracted from each other. White lines mark significant genotype differences ($P=0.05$). Note that activity in the inter-δ/θ band is increased more in CKO mice than in CTR, in particular in the 2nd half of the SD. θ frequency narrowing and acceleration, as well as activity in the 70-90 Hz range, are reduced in CKO relative to CTR, in particular in the 1st half of the SD. Importantly, note that the color codes for (**c**) and (**d**) differ in the code indicating 'no change': in (**c**), a 100% reference value is coded as dark-blue. In (**d**), a zero value (CKO=CTR) is coded as light-green. (**d**) Time-course of ECoG power within specific frequency ranges are plotted across time relative to its mean value in baseline ZT8-12 wakefulness [%].

Fig. 5. Nesting-associated waking displays a more pronounced θ rhythm, and higher fast-γ power in *Hcrtr1*$^{Dbh\text{-}CKO}$ relative to *Hcrtr1*$^{Dbh\text{-}CTR}$ littermates, as well as induction of β/slow-γ activities. Nest material (a Nestlet^{TM}) was added at dark onset (ZT12), and the ECoG recorded in the following 24h. (**a-b**) ECoG spectra of wakefulness during the last 6h (**a**, ZT18-24), or 2h (**b**, ZT22-24) of the nesting night are plotted as % of the baseline total power reference [%], as in Fig. 3d-e. (**c-d**) Waking ECoG spectral profiles in the last 6h (**c**), or last 2h (**d**) of the nesting night are contrasted to waking in the same time interval in baseline. The ECoG power ratio is depicted as $\log_2$ of its value. A value of 0 indicates no change, and a value of +1 or -1 indicates a 2-fold change. Red bars indicate significant genotype differences between genotypes (two-way ANOVA, followed by post-hoc independent two-tailed student *t*-test, $p<0.05$). (**e**) Heatmaps representing the waking spectral dynamics across the nesting night and the following

light phase were constructed as for the B1-B2-SD-day recording shown in Fig. 4a. Plotted are ECoG power densities for each 0.25 Hz frequency bin relative to their values in wakefulness of baseline (B1+B2) ZT8-12 periods [%]. (**g**) A differential CKO-CTR heatmap of the nesting 24h period was constructed similarly to Fig. 4g for the B1-B2-SD recording. Note that the color code for (**e**) and (**g**) differ. In (**e**), 100% reference value is coded as dark-blue. In (**g**), a zero value (CKO=CTR) is coded as light-green. (**f**) Time-courses of time-spent-awake [min/h]. Red bar indicates significant genotype differences between genotypes (two-way ANOVA, followed by post-hoc independent two-tailed student *t*-test, $p<0.05$).

Fig. 6. **Electrocortical responses to cage change (CC).** Mice were removed from their nesting cage at ZT3 of the 9th recording day and transferred to a fresh cage. (**a** top) Waking ECoG spectra from CC to SWS-onset in *Hcrtr1*$^{Dbh\text{-}CKO}$ (CKO, n=8), and *Hcrtr1*$^{Dbh\text{-}CTR}$ (CTR, n=6) mice. Plotted are power density values, expressed as percentage of each animal's total ECoG power (see Methods). Note the non-linear axes. (**a** bottom) ECoG power density ratio of post-CC waking relative to average waking in the preceding 24h period (day 8) [$\log_2$ of ratio]. Red bars indicate significant genotype differences (two-way ANOVA, followed by post-hoc independent two-tailed student *t*-test, $P<0.05$). (**b**) Latencies to SWS-onset tended to be shorter in CKO than CTR mice. (**c**). Spectral dynamics of the waking ECoG after cage change, across time (ZT3 to SWS-onset), frequencies (0.75 -90.0 Hz), and power (as % of each mouse' mean waking ECoG power in that frequency bin in the preceding day's ZT8-12 time interval; plotted as $\log_2$ value and color-coded as shown on the right). x-axis shows ZT time, adjusted to individual waking latencies to SWS-onset. (**d**) Differential CKO-CTR waking power dynamics are shown, similarly as in Fig. 4c and Fig. 5g. Note that the color code for (**c**) and (**d**) differ. In (**c**), 100% reference value is coded as dark-blue. In (**d**), a zero value (CKO=CTR) is coded as light-green. (**e**) Time-courses of waking ECoG power over the CC-to-SWS-onset waking period within specific frequency ranges that showed modulation in **c-d** (3.5-6.0 Hz; 7.5-11.5 Hz; 65-75 Hz). Red stars, significant genotype differences (independent two-tailed student *t*-test, $p<0.05$). Black star, marginally significant genotype difference (independent two-tailed student *t*-test, $P=0.051$).

Fig. 7. **Slow-wave-sleep of *Hcrtr1*$^{Dbh\text{-}CKO}$ mice is deficient in slow-δ (δ1: 0.75-2.00 Hz) oscillations, in particular following active waking periods.** (**a-d**) ECoG power spectra across 0.75-40.0 Hz (**a**) in baseline SWS (BL1+BL2), (**c**) the first 20 min of SWS following light-onset in baseline, (**b**) the first 20 min of SWS following SD, and (**d**) the first 20 min of SWS following CC-induced waking. Plotted are power values referenced to each animal's baseline total ECoG power value [%]. Vertical guides indicate the 0.75 Hz, 2.5 Hz and 4.25 Hz frequencies, delineating two subranges of δ oscillations (δ1: 0.75-2.00 Hz; δ2: 2.50-4.25 Hz). All 4 SWS analyses show significant genotype differences and genotype x frequency interactions (2-Way ANOVA for Genotype and Frequency x Genotype interaction; $P<0.01$). *Hcrtr1*$^{Dbh\text{-}CKO}$ (CKO) mice

show a selective deficit in slow-δ, relative to *Hcrtr1*$^{Dbh\text{-}CTR}$ (CTR) littermates, with genotype differences becoming more pronounced under high sleep pressure, i.e. in dark phase, post-SD and post-CC SWS. (**e**) To emphasize genotype effects, SWS spectra of *Hcrtr1*$^{Dbh\text{-}CKO}$ mice in distinct experimental contexts are referenced to spectra of *Hcrtr1*$^{Dbh\text{-}CTR}$ mice littermates in the same contexts. The resulting CKO/CTR ECoG power ratio spectral distribution shows that CKO mice' spectra differ most from CTR mice' spectra in the slow-δ band, and post-SD and post-CC SWS resemble each other the most in their response to Hcrt-to-NA lesioning.

Fig. 8. Dynamics of slow-δ (0.75-2.0) and fast-δ (2.5-4.25) power in SWS of *Hcrtr1*$^{Dbh\text{-}CKO}$ and *Hcrtr1*$^{Dbh\text{-}CTR}$ mice in B1-B2-SD and CC experimental contexts. ECoG δ power is plotted as % of baseline total ECoG power calculated for each mouse across all frequencies, and all states (see Methods). Slow-δ CKO values are inferior to CTR values at all times, and most significantly so following maximal waking periods, such as after SD (**b**) , or after CC-induced waking (**e**).

Fig. S1. Interpreting spectral power dynamic plots: maxima in ECoG power ratio spectra do not represent peaks of ECoG oscillatory activity. To contrast two power spectra, or to depict a spectral profile relative to another (reference) spectral profile (e.g. ECoG waking spectrum during SD vs. waking spectrum in baseline), the ratio of the two spectra can be plotted as a spectral distribution which should be interpreted with caution: a peak in this spectral distribution represents a frequency at which the two spectra differ maximally. This peak should not be confused with the peak of the oscillations on which the two spectra being compared are based. Illustrating this, the mean ECoG power spectrum during SD-wakefulness is shown in color, and the reference waking spectrum to which it is contrasted (reference), i.e. waking in the last 4h of baseline light phase (BL ZT8-12) is shown in grey. (Here, mean spectra of n=7 *Hcrtr1*$^{Dbh\text{-}CTR}$ mice are depicted as an example). SD induces the emergence of a sharp θ rhythm, with a peak frequency at 8.5 Hz. (**b**) depicts the ECoG power ratio between these two spectra, revealing a peak at 9.25 Hz, the frequency at which the two spectra differ the most. This peak does not evidence any 9.25 Hz brain oscillation.

References

Adamantidis AR, Zhang F, Aravanis AM, Deisseroth K, de Lecea L. 2007. Neural substrates of awakening probed with optogenetic control of hypocretin neurons. *Nature* 450: 420-424.

Aeschbach D, Matthews JR, Postolache TT, Jackson MA, Giesen HA, Wehr TA. 1997. Dynamics of the human EEG during prolonged wakefulness: evidence for frequency-specific circadian and homeostatic influences. *Neuroscience letters* 239: 121-124.

Baldo BA, Daniel RA, Berridge CW, Kelley AE. 2003. Overlapping distributions of orexin/hypocretin- and dopamine-beta-hydroxylase immunoreactive fibers in rat brain regions mediating arousal, motivation, and stress. *The Journal of comparative neurology* 464: 220-237.

Berridge CW. 2008. Noradrenergic modulation of arousal. *Brain Res Rev* 58: 1-17.

Berridge CW, Espana RA. 2000. Synergistic sedative effects of noradrenergic alpha(1)- and beta-receptor blockade on forebrain electroencephalographic and behavioral indices. *Neuroscience* 99: 495-505.

Berridge CW, Foote SL. 1991. Effects of Locus-Coeruleus Activation on Electroencephalographic Activity in Neocortex and Hippocampus. *Journal of Neuroscience* 11: 3135-3145.

Brown RA, Walling SG, Milway JS, Harley CW. 2005. Locus ceruleus activation suppresses feedforward interneurons and reduces beta-gamma electroencephalogram frequencies while it enhances theta frequencies in rat dentate gyrus. *The Journal of neuroscience* 25: 1985-1991.

Buzsaki G. 2002. Theta oscillations in the hippocampus. *Neuron* 33: 325-340.

Cajochen C, Brunner DP, Krauchi K, Graw P, Wirz-Justice A. 1995. Power density in theta/alpha frequencies of the waking EEG progressively increases during sustained wakefulness. *Sleep* 18: 890-894.

Cajochen C, Wyatt JK, Czeisler CA, Dijk DJ. 2002. Separation of circadian and wake duration-dependent modulation of EEG activation during wakefulness. *Neuroscience* 114: 1047-1060.

Carter ME, Brill J, Bonnavion P, Huguenard JR, Huerta R, de Lecea L. 2012. Mechanism for Hypocretin-mediated sleep-to-wake transitions. *Proceedings of the National Academy of Sciences of the United States of America* 109: E2635-2644.

Carter ME, Yizhar O, Chikahisa S, Nguyen H, Adamantidis A, Nishino S, Deisseroth K, de Lecea L. 2010. Tuning arousal with optogenetic modulation of locus coeruleus neurons. *Nature neuroscience* 13: 1526-1533.

Ch'ng SS, Lawrence AJ. 2015. Distribution of the orexin-1 receptor (OX1R) in the mouse forebrain and rostral brainstem: A characterisation of OX1R-eGFP mice. *Journal of chemical neuroanatomy* 66-67: 1-9.

Chemelli RM, Willie JT, Sinton CM, Elmquist JK, Scammell T, Lee C, Richardson JA, Williams SC, Xiong Y, Kisanuki Y et al. 1999. Narcolepsy in orexin knockout mice: molecular genetics of sleep regulation. *Cell* 98: 437-451.

Cirelli C, Gutierrez CM, Tononi G. 2004. Extensive and divergent effects of sleep and wakefulness on brain gene expression. *Neuron* 41: 35-43.

Cirelli C, Huber R, Gopalakrishnan A, Southard TL, Tononi G. 2005. Locus ceruleus control of slow-wave homeostasis. *The Journal of neuroscience* 25: 4503-4511.

Cutler DJ, Morris R, Sheridhar V, Wattam TA, Holmes S, Patel S, Arch JR, Wilson S, Buckingham RE, Evans ML et al. 1999. Differential distribution of orexin-A and orexin-B immunoreactivity in the rat brain and spinal cord. *Peptides* 20: 1455-1470.

Darwinkel A, Stanic D, Booth LC, May CN, Lawrence AJ, Yao ST. 2014. Distribution of Orexin-1 Receptor-Green Fluorescent Protein- (Ox1-Gfp) Expressing Neurons in the Mouse Brain Stem and Pons: Co-Localization with Tyrosine Hydroxylase and Neuronal Nitric Oxide Synthase. *Neuroscience* 278: 253-264.

Delaville C, McCoy AJ, Gerber CM, Cruz AV, Walters JR. 2015. Subthalamic nucleus activity in the awake hemiparkinsonian rat: relationships with motor and cognitive networks. *The Journal of neuroscience* 35: 6918-6930.

Devilbiss DM, Waterhouse BD. 2011. Phasic and Tonic Patterns of Locus Coeruleus Output Differentially Modulate Sensory Network Function in the Awake Rat. *Journal of neurophysiology* 105: 69-87.

Dijk DJ, Duffy JF, Czeisler CA. 1992. Circadian and Sleep Wake Dependent Aspects of Subjective Alertness and Cognitive Performance. *Journal of sleep research* 1: 112-117.

Dzirasa K, Phillips HW, Sotnikova TD, Salahpour A, Kumar S, Gainetdinov RR, Caron MG, Nicolelis MA. 2010. Noradrenergic control of cortico-striato-thalamic and mesolimbic cross-structural synchrony. *The Journal of neuroscience* 30: 6387-6397.

Eban-Rothschild A, Rothschild G, Giardino WJ, Jones JR, de Lecea L. 2016. VTA dopaminergic neurons regulate ethologically relevant sleep-wake behaviors. *Nature neuroscience*.

Engel AK, Fries P. 2010. Beta-band oscillations--signalling the status quo? *Current opinion in neurobiology* 20: 156-165.

Finelli LA, Baumann H, Borbely AA, Achermann P. 2000. Dual electroencephalogram markers of human sleep homeostasis: correlation between theta activity in waking and slow-wave activity in sleep. *Neuroscience* 101: 523-529.

Flores A, Valls-Comamala V, Costa G, Saravia R, Maldonado R, Berrendero F. 2014. The Hypocretin/Orexin System Mediates the Extinction of Fear Memories. *Neuropsychopharmacology* 39: 2732-2741.

Foote SL, Astonjones G, Bloom FE. 1980. Impulse Activity of Locus Coeruleus Neurons in Awake Rats and Monkeys Is a Function of Sensory Stimulation and Arousal. *P Natl Acad Sci-Biol* 77: 3033-3037.

Franken P, Dijk DJ, Tobler I, Borbely AA. 1991a. Sleep deprivation in rats: effects on EEG power spectra, vigilance states, and cortical temperature. *The American journal of physiology* 261: R198-208.

Franken P, Malafosse A, Tafti M. 1998. Genetic variation in EEG activity during sleep in inbred mice. *The American journal of physiology* 275: R1127-1137.

Franken P, Tobler I, Borbely AA. 1991b. Sleep homeostasis in the rat: simulation of the time course of EEG slow-wave activity. *Neuroscience letters* 130: 141-144.

Gaskill BN, Karas AZ, Garner JP, Pritchett-Corning KR. 2013. Nest Building as an Indicator of Health and Welfare in Laboratory Mice. *Jove-J Vis Exp*.

Hagan JJ, Leslie RA, Patel S, Evans ML, Wattam TA, Holmes S, Benham CD, Taylor SG, Routledge C, Hemmati P et al. 1999. Orexin A activates locus coeruleus cell firing and increases arousal in the rat. *Proceedings of the National Academy of Sciences of the United States of America* 96: 10911-10916.

Hammond C, Bergman H, Brown P. 2007. Pathological synchronization in Parkinson's disease: networks, models and treatments. *Trends in neurosciences* 30: 357-364.

Hasan S, Pradervand S, Ahnaou A, Drinkenburg W, Tafti M, Franken P. 2009. How to keep the brain awake? The complex molecular pharmacogenetics of wake promotion. *Neuropsychopharmacology* 34: 1625-1640.

Hasegawa E, Yanagisawa M, Sakurai T, Mieda M. 2014. Orexin neurons suppress narcolepsy via 2 distinct efferent pathways. *J Clin Invest* 124: 604-616.

Horvath TL, Peyron C, Diano S, Ivanov A, Aston-Jones G, Kilduff TS, van Den Pol AN. 1999. Hypocretin (orexin) activation and synaptic innervation of the locus coeruleus noradrenergic system. *The Journal of comparative neurology* 415: 145-159.

Huber R, Deboer T, Tobler I. 2000. Topography of EEG dynamics after sleep deprivation in mice. *Journal of neurophysiology* 84: 1888-1893.

Hunsley MS, Curtis WR, Palmiter RD. 2006. Behavioral and sleep/wake characteristics of mice lacking norepinephrine and hypocretin. *Genes, brain, and behavior* 5: 451-457.

Jenkinson N, Brown P. 2011. New insights into the relationship between dopamine, beta oscillations and motor function. *Trends in neurosciences* 34: 611-618.

Lal SK, Craig A. 2001. A critical review of the psychophysiology of driver fatigue. *Biological psychology* 55: 173-194.

Lal SKL, Craig A. 2002. Driver fatigue: Electroencephalography and psychological assessment. *Psychophysiology* 39: 313-321.

Larson J, Wong D, Lynch G. 1986. Patterned stimulation at the theta frequency is optimal for the induction of hippocampal long-term potentiation. *Brain research* 368: 347-350.

Lemaire N, Hernandez LF, Hu D, Kubota Y, Howe MW, Graybiel AM. 2012. Effects of dopamine depletion on LFP oscillations in striatum are task- and learning-dependent and selectively reversed by L-DOPA. *Proceedings of the National Academy of Sciences of the United States of America* 109: 18126-18131.

Lin L, Faraco J, Li R, Kadotani H, Rogers W, Lin X, Qiu X, de Jong PJ, Nishino S, Mignot E. 1999. The sleep disorder canine narcolepsy is caused by a mutation in the hypocretin (orexin) receptor 2 gene. *Cell* 98: 365-376.

Mang GM, Franken P. 2012. Sleep and EEG Phenotyping in Mice. *Current protocols in mouse biology* 2: 55-74.

Mang GM, La Spada F, Emmenegger Y, Chappuis S, Ripperger JA, Albrecht U, Franken P. 2016. Altered Sleep Homeostasis in Rev-erbalpha Knockout Mice. *Sleep* 39: 589-601.

Marcus JN, Aschkenasi CJ, Lee CE, Chemelli RM, Saper CB, Yanagisawa M, Elmquist JK. 2001. Differential expression of orexin receptors 1 and 2 in the rat brain. *The Journal of comparative neurology* 435: 6-25.

McFarland WL, Teitelbaum H, Hedges EK. 1975. Relationship between hippocampal theta activity and running speed in the rat. *Journal of comparative and physiological psychology* 88: 324-328.

McGinley MJ, Vinck M, Reimer J, Batista-Brito R, Zagha E, Cadwell CR, Tolias AS, Cardin JA, McCormick DA. 2015. Waking State: Rapid Variations Modulate Neural and Behavioral Responses. *Neuron* 87: 1143-1161.

Nishino S, Mignot E. 1997. Pharmacological aspects of human and canine narcolepsy. *Progress in neurobiology* 52: 27-78.

Parlato R, Otto C, Begus Y, Stotz S, Schutz G. 2007. Specific ablation of the transcription factor CREB in sympathetic neurons surprisingly protects against developmentally regulated apoptosis. *Development* 134: 1663-1670.

Peyron C, Tighe DK, van den Pol AN, de Lecea L, Heller HC, Sutcliffe JG, Kilduff TS. 1998. Neurons containing hypocretin (orexin) project to multiple neuronal systems. *The Journal of neuroscience* 18: 9996-10015.

Phipps-Nelson J, Redman JR, Rajaratnam SM. 2011. Temporal profile of prolonged, night-time driving performance: breaks from driving temporarily reduce time-on-task fatigue but not sleepiness. *Journal of sleep research* 20: 404-415.

Puskas N, Papp RS, Gallatz K, Palkovits M. 2010. Interactions between orexin-immunoreactive fibers and adrenaline or noradrenaline-expressing neurons of the lower brainstem in rats and mice. *Peptides* 31: 1589-1597.

Sebban C, Zhang XQ, Tesolin-Decros B, Millan MJ, Spedding M. 1999. Changes in EEG spectral power in the prefrontal cortex of conscious rats elicited by drugs interacting with dopaminergic and noradrenergic transmission. *British journal of pharmacology* 128: 1045-1054.

Singh C, Oikonomou G, Prober DA. 2015. Norepinephrine is required to promote wakefulness and for hypocretin-induced arousal in zebrafish. *eLife* 4: e07000.

Slawinska U, Kasicki S. 1998. The frequency of rat's hippocampal theta rhythm is related to the speed of locomotion. *Brain research* 796: 327-331.

Soya S, Shoji H, Hasegawa E, Hondo M, Miyakawa T, Yanagisawa M, Mieda M, Sakurai T. 2013. Orexin receptor-1 in the locus coeruleus plays an important role in cue-dependent fear memory consolidation. *The Journal of neuroscience* 33: 14549-14557.

Trivedi P, Yu H, MacNeil DJ, Van der Ploeg LH, Guan XM. 1998. Distribution of orexin receptor mRNA in the rat brain. *FEBS letters* 438: 71-75.

Vassalli A, Dellepiane JM, Emmenegger Y, Jimenez S, Vandi S, Plazzi G, Franken P, Tafti M. 2013. Electroencephalogram paroxysmal theta characterizes cataplexy in mice and children. *Brain : a journal of neurology* 136: 1592-1608.

Vassalli & Franken. Hypocretin (Orexin) is critical in sustaining theta/gamma-rich waking behaviors: implications for the sleep homeostatic process. *Manuscript in revision*.

Vassalli A, Li S, Tafti M. 2015. Comment on "Antibodies to influenza nucleoprotein cross-react with human hypocretin receptor 2". *Science translational medicine* 7: 314le312.

Vazey EM, Aston-Jones G. 2014. Designer receptor manipulations reveal a role of the locus coeruleus noradrenergic system in isoflurane general anesthesia. *Proceedings of the National Academy of Sciences of the United States of America* 111: 3859-3864.

Vyazovskiy VV, Tobler I. 2005. Theta activity in the waking EEG is a marker of sleep propensity in the rat. *Brain research* 1050: 64-71.

Walling SG, Brown RA, Milway JS, Earle AG, Harley CW. 2011. Selective tuning of hippocampal oscillations by phasic locus coeruleus activation in awake male rats. *Hippocampus* 21: 1250-1262.

Walling SG, Nutt DJ, Lalies MD, Harley CW. 2004. Orexin-A infusion in the locus ceruleus triggers norepinephrine (NE) release and NE-induced long-term potentiation in the dentate gyrus. *The Journal of neuroscience* 24: 7421-7426.

Acknowledgements

A. V. wants to thank Paul Feinstein and the late Andrea Waltz for advice in gene targeting strategy. We thank Christina Schrick and Yann Emmenegger for superb technical assistance, Arnaud Paradis for help in confocal microscopy, and Mehdi Tafti for his critical insight.

Author Contributions

A.V. designed and generated the *Hcrtr1*^{flox} and *Hcrtr1*$^{\Delta\text{-}Gfp}$ alleles and designed the project; S.L. performed the mice experimentation and analysis; P.F. elaborated the ECoG analysis methods and performed analysis. A.V. wrote the paper and all authors reviewed the manuscript.

Additional Information

Competing financial interests: The authors declare no competing financial interests.

Abbreviations: CC: cage change; CKO: conditional knockout; CTR: control; *Dbh*: dopamine beta-hydroxylase; ECoG: electrocorticogram; EMG: electromyogram; GFP: green fluorescent protein; *Hcrtr1*: hypocretin receptor 1; *Hcrtr2*: hypocretin receptor 2; LC: locus coeruleus; NA: noradrenaline; PS: paradoxical sleep; SD: sleep deprivation; SWS: slow wave sleep; TPF: θ peak frequency; TH: tyrosine hydroxylase; W: wakefulness; ZT: zeitgeber.

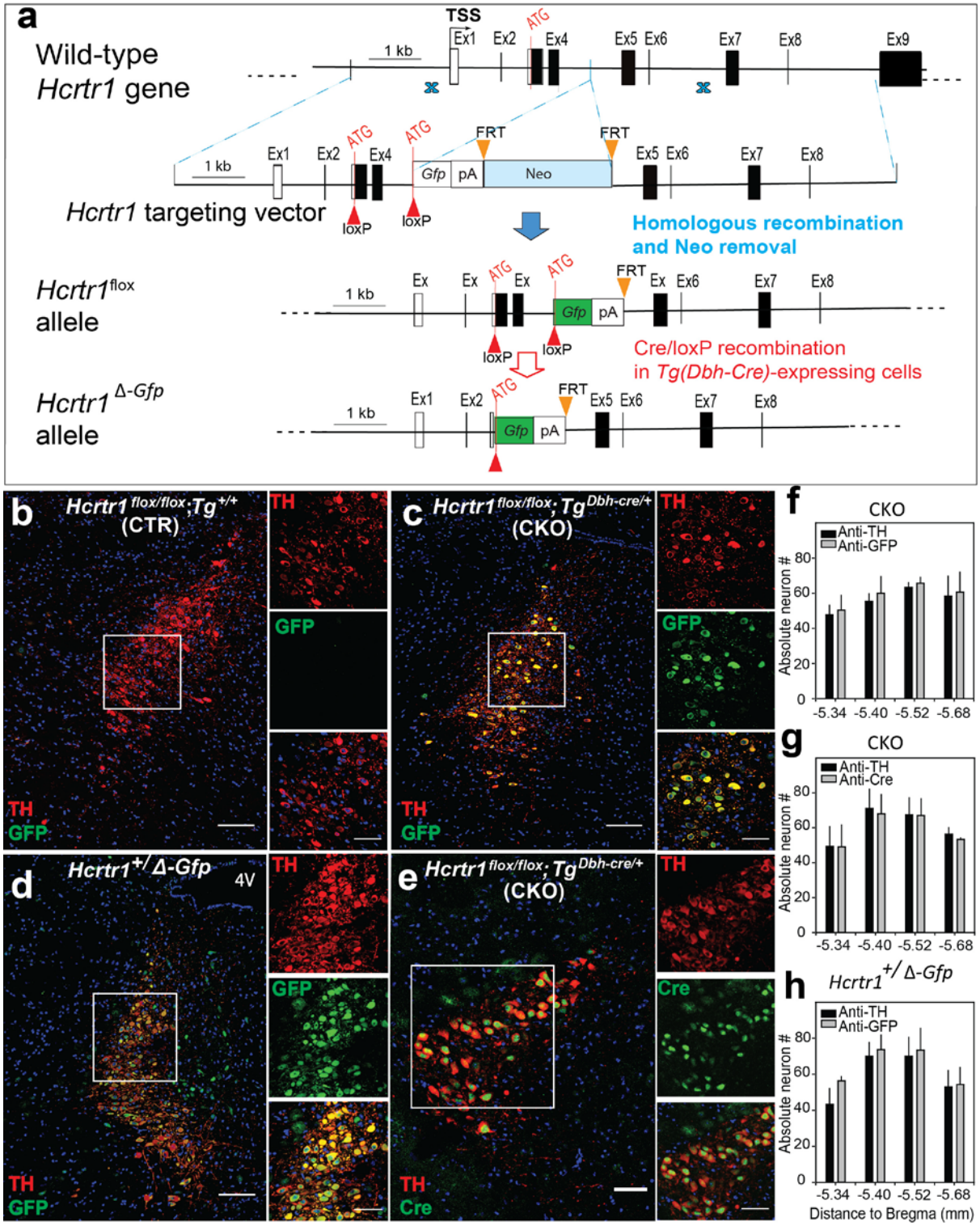

Figure 1

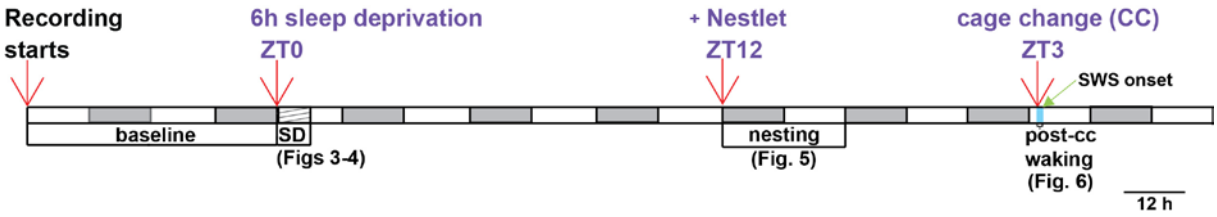

Figure 2

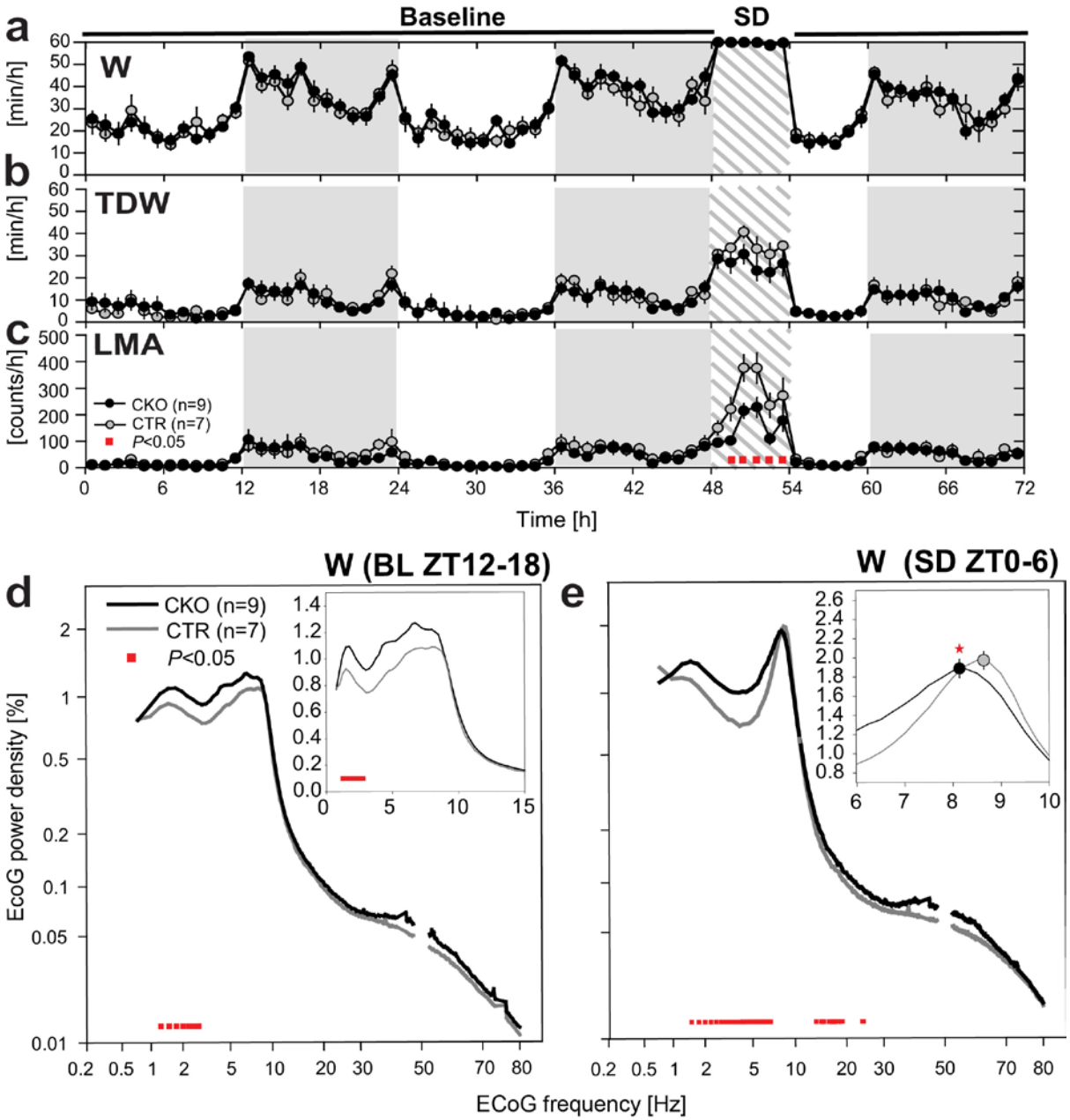

Figure 3

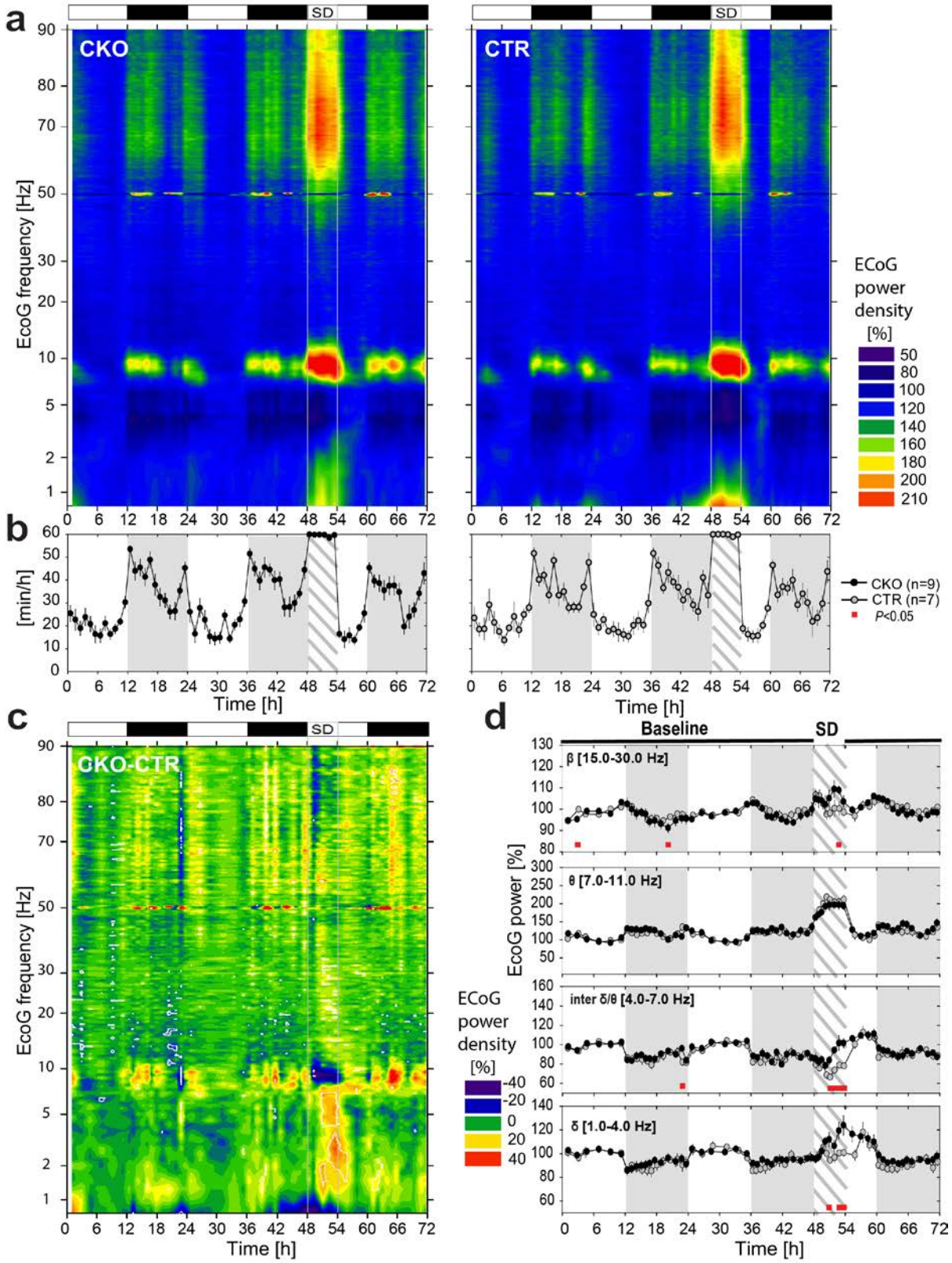

Figure 4

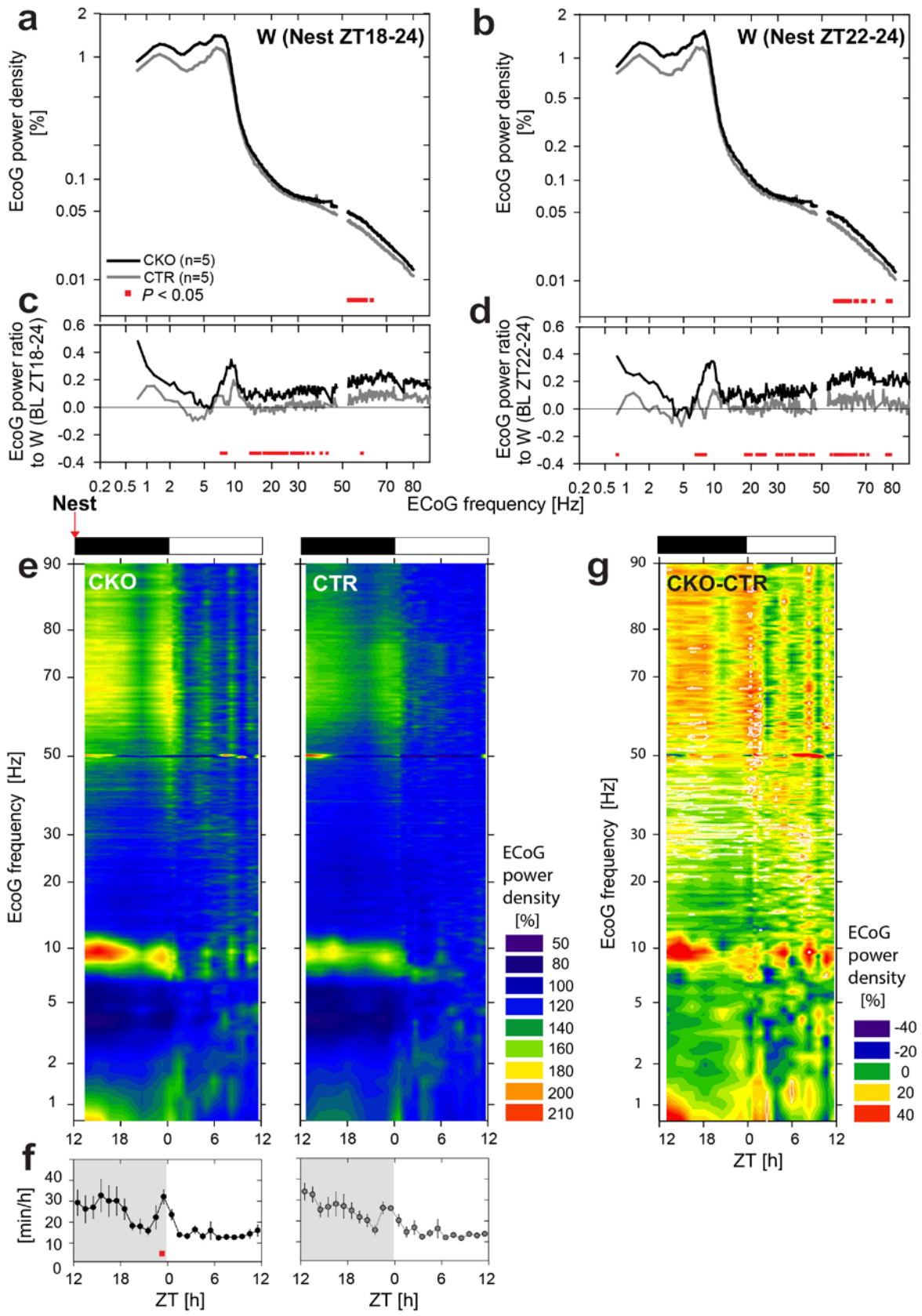

Figure 5

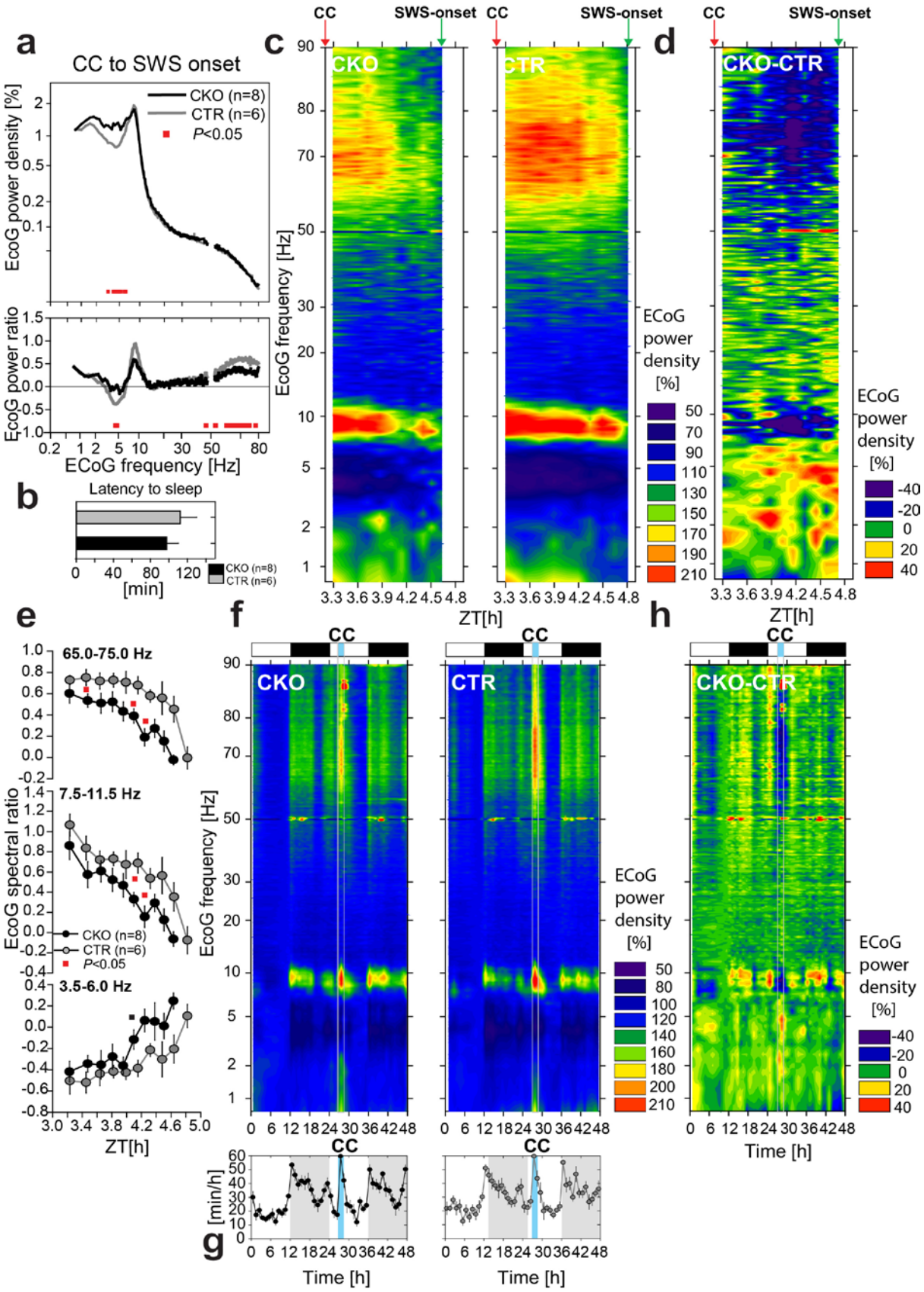

Figure 6

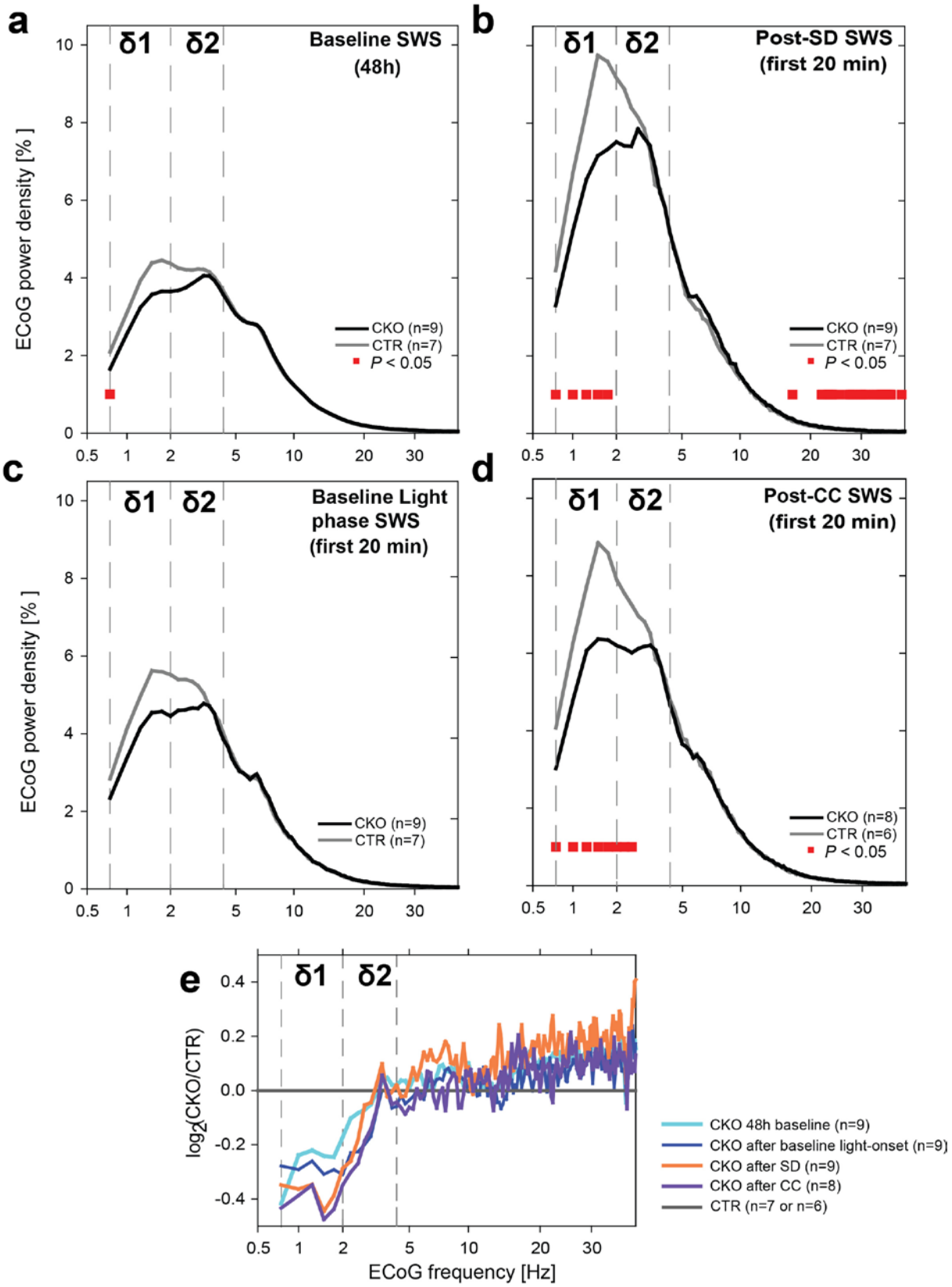

Figure 7

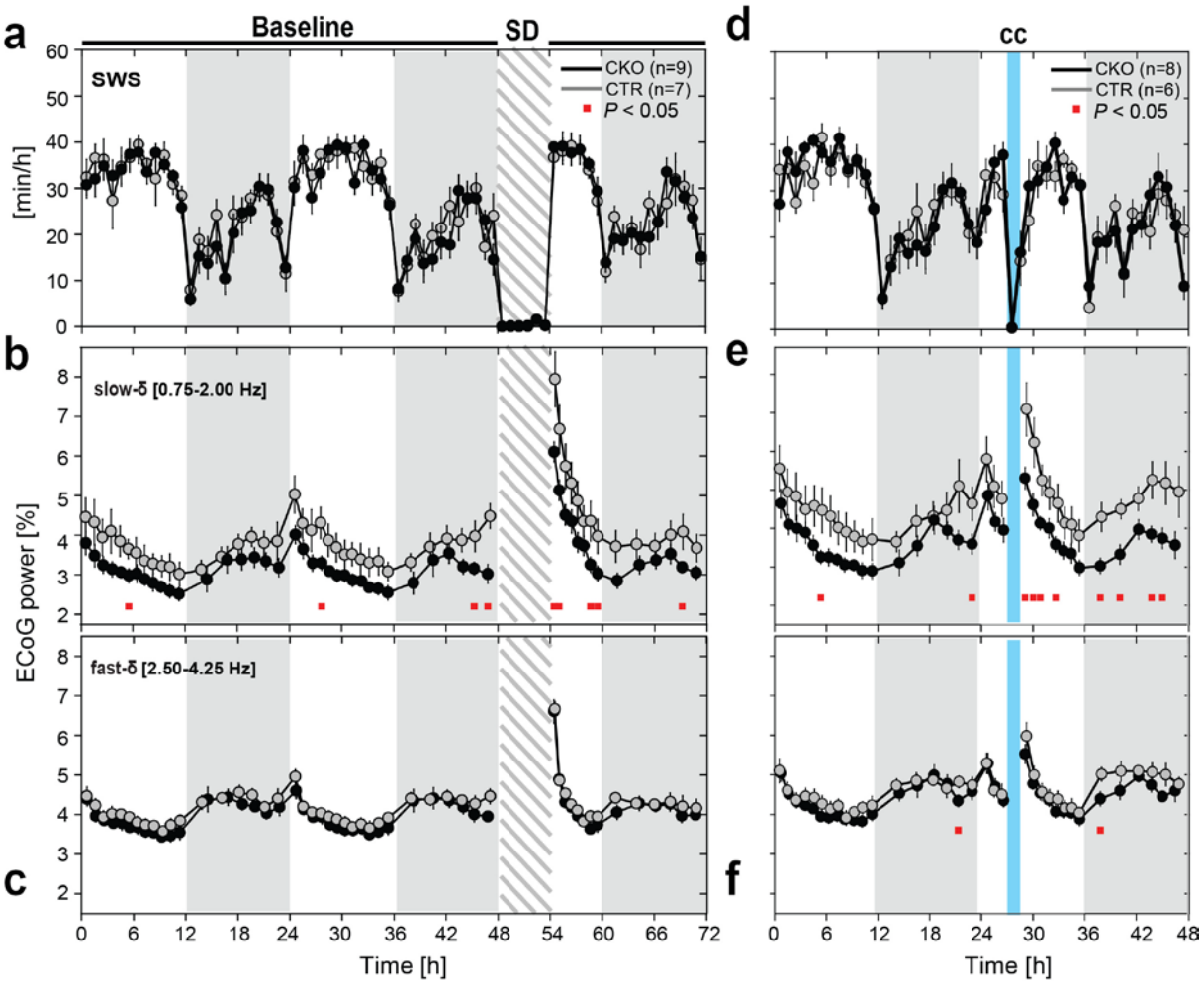

Figure 8

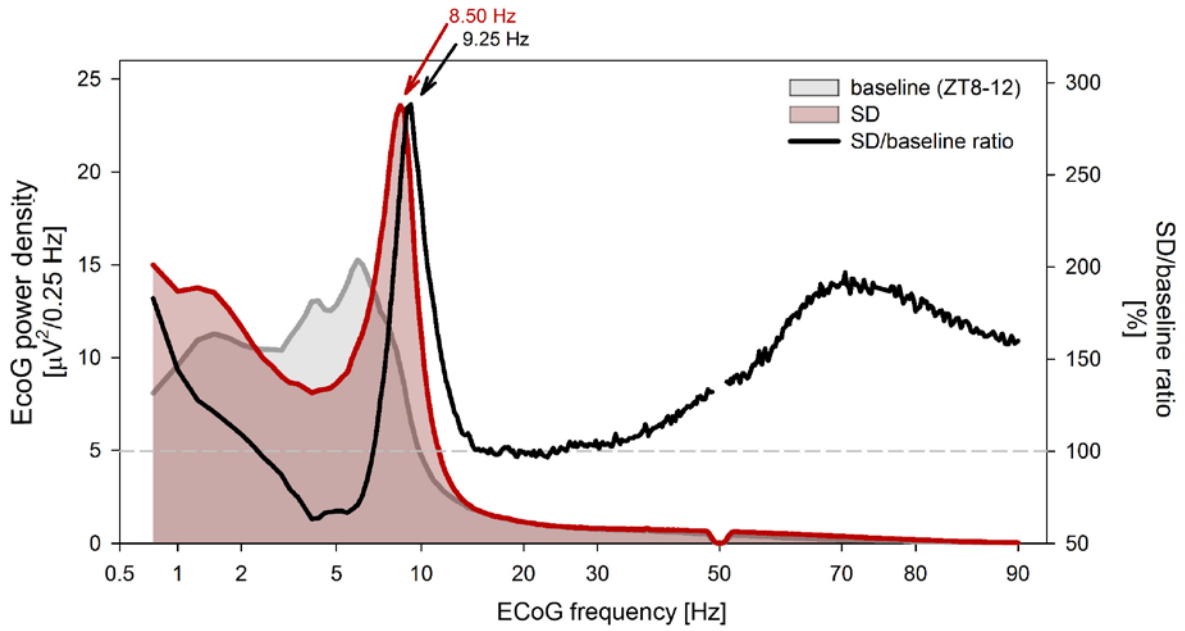

Figure S1

Suppl. Table 1.

Behavioral state distribution in days 1 to 3 of recording (48h baseline, followed by 6h SD and recovery). Time spent in W, SWS and PS (mean±SEM).

	Baseline				SD-day		
	W (min)	**SWS (min)**	**PS (min)**		**W (min)**	**SWS (min)**	**PS (min)**
24h light+dark				**24h light+dark**			
CTR (n=7)	701.85±25.21	658.35±23.30	79.80±4.69	CTR (n=7)	878.05±16.73	487.70±14.26	74.26±3.61
CKO (n=9)	720.72±24.31	634.59±22.93	84.7±3.12	CKO (n=9)	879.13±23.85	486.18±21.45	74.70±3.75
12h light phase				**Recovery 6h light**			
CTR (n=7)	250.23±10.55	412.91±10.04	56.77±2.75	CTR (n=7)	114.00±6.77	213.28±6.14	23.72±1.68
CKO (n=9)	251.03±10.30	406.27±9.18	62.70±2.66	CKO (n=9)	104.80±7.34	218.67±6.26	36.53±2.02
12h dark phase				**12h dark phase**			
CTR (n=7)	451.53±17.77	245.44±16.42	23.03±2.54	CTR (n=7)	405.46±16.44	273.01±13.57	41.53±2.85
CKO (n=9)	469.69±16.99	228.31±15.64	22.00±1.98	CKO (n=9)	416.96±4.74	265.12±15.75	38.17±2.53

Suppl. Table 2.

Peak frequency of the θ rhythm (TPF) expressed in wakefulness as *Hcrtr1*$^{Dbh\text{-}CKO}$ and *Hcrtr1*$^{Dbh\text{-}CTR}$ mice experiment different behavioral contexts. Mean±SEM. TDW, θ-dominated-wakefulness. * indicates significant difference between genotypes (independent *t*-test, $P<0.05$).

	Theta Peak Frequency [Hz] ***Hcrtr1*$^{Dbh\text{-}CKO}$ vs. *Hcrtr1*$^{Dbh\text{-}CTR}$**
Baseline (48h) TDW	7.86±0.11 vs. 8.07±0.11
6h SD wakefulness	8.14±0.09 vs. 8.57±0.11*
Post-CC wakefulness	7.70±0.33 vs. 8.10±0.15

Suppl. Methods.

Mice. Mice were in a mixed *C57BL/6NTac* x *C57BL/6J* background. It is noteworthy that the 2 strains differ significantly in sleep/wake parameters. Notably, we found that *C57BL/6NTac* spend less time awake than *C57BL/6J* mice (50.57±1.24 % wakefulness, 43.74 ± 1.14% SWS; 5.69± 0.27% PS, n=8 for *C57BL/6NTac* mice and 54.86± 1.14% wakefulness, 40.25± 1.12% SWS; 4.89± 0.21% PS, n=11 for *C57BL/6J* mice. W: t_{17}= 2.520, *P*= 0.02; SWS: t_{17}= -2.129, *P*= 0.048; PS: t_{17}= -2.332, *P*=0.03, by unpaired two-tailed Student's *t* tests).